

Lawrence Berkeley National Laboratory

LBL Publications

Title

Thermal Decompositions of the Lignin Model Compounds: Salicylaldehyde and Catechol

Permalink

<https://escholarship.org/uc/item/52t6c0mz>

Journal

The Journal of Physical Chemistry A, 122(28)

ISSN

1089-5639

Authors

Ormond, Thomas K

Baraban, Joshua H

Porterfield, Jessica P

et al.

Publication Date

2018-07-19

DOI

10.1021/acs.jpca.8b03201

Peer reviewed

Thermal Decompositions of the Lignin Model Compounds: Salicylaldehyde and Catechol

Thomas K. Ormond,^{1,2} Joshua H. Baraban,^{2,3} Jessica P. Porterfield,^{2,4} Adam M. Scheer,^{5,6} Patrick Hemberger,⁷ Tyler P. Troy,⁸ Musahid Ahmed,⁸ Mark R. Nimlos,¹ David J. Robichaud,¹ John W. Daily,⁹ and G. Barney Ellison²

1. National Renewable Energy Laboratory, 15013 Denver West Parkway, Golden CO, 80401, U.S.A.
2. Department of Chemistry and Biochemistry, University of Colorado, Boulder, 80309-0215, U.S.A.
3. Present address: Department of Chemistry, Ben Gurion University of the Negev, Beer Sheva, Israel 84105
4. Present address: Harvard-Smithsonian Center for Astrophysics, Cambridge, MA 02138
5. Combustion Research Facility, Sandia National Laboratory, PO Box 969, Livermore, CA 94551-0969, U.S.A.
6. Present address: Pacific Gas and Electric Company, 245 Market St., San Francisco, CA 94111
7. Laboratory for Femtochemistry and Synchrotron Radiation, Paul Scherrer Institute, CH-5234 Villigen-PSI, Switzerland
8. Chemical Sciences Division, Lawrence Berkeley National Laboratories, Berkeley, CA 94720, U.S.A.
9. Center for Combustion and Environmental Research, Department of Mechanical Engineering, University of Colorado, Boulder, CO 80309-0427, U.S.A.

Abstract

The nascent steps in the pyrolysis of the lignin components, salicylaldehyde (*o*-HOC₆H₄CHO) and catechol (*o*-HOC₆H₄OH), have been studied in a set of heated micro-reactors. The micro-reactors are small (roughly 1 mm ID x 3 cm long); transit times through the reactors are about 100 μ sec. Temperatures in the micro-reactors can be as high as 1600 K and pressures are typically a few hundred Torr. The products of pyrolysis are identified by a combination of photoionization mass spectrometry, photoelectron photoion coincidence mass spectroscopy, and matrix isolation infrared spectroscopy. The main pathway by which salicylaldehyde decomposes is a concerted fragmentation: *o*-HOC₆H₄CHO (+ M) \rightarrow H₂ + CO + C₅H₄=C=O (fulveneketene). At temperatures above 1300 K, fulveneketene loses CO to yield a mixture of (HC \equiv C-C \equiv C-CH₃, HC \equiv C-CH₂-C \equiv CH, and HC \equiv C-CH=C=CH₂). These alkynes decompose to a mixture of radicals (HC \equiv C-C \equiv C-CH₂ and HC \equiv C-CH-C \equiv CH) and H-atoms. H-atom chain reactions convert salicylaldehyde to phenol: *o*-HOC₆H₄CHO + H \rightarrow C₆H₅OH + CO + H. Catechol has similar chemistry to salicylaldehyde. Electrocyclic fragmentation produces water and fulveneketene: *o*-HOC₆H₄OH (+ M) \rightarrow H₂O + C₅H₄=C=O. These findings have implications for the pyrolysis of lignin itself.

(Revised to J. Phys. Chem. A, June 2018)

I. Introduction

Lignocellulosic biomass, an abundant and renewable resource,¹ is a complex amalgam of three classes of biopolymers: cellulose, hemicelluloses, and lignin. This paper examines the pyrolysis of two common lignin components, salicylaldehyde (*o*-HOC₆H₄CHO) and catechol (*o*-HOC₆H₄OH). Both of these species are important thermal decomposition products² in the conversion of lignins to biofuels. The development of biomass derived fuels^{3,4} as an alternative to petroleum-based fuels has become a topic of interest due to climate change⁵ and availability of this raw biomass. Biomass is the only renewable source of carbon-based fuels and platform organic chemicals.

After cellulose, lignin⁶ is the second most abundant terrestrial biopolymer, accounting for roughly one third of the organic carbon in the biosphere.⁷ Lignin is a complex, water-insoluble aromatic polymer and a representative structure is shown in Scheme 1 (adapted from Fig. 2 of ref. ⁸). Lignin is essential for the structural integrity of the cell wall and the stiffness and strength of the stem. Besides waterproofing the cell wall, lignin enables the transport of water and solutes through the vascular system and plays a role in protecting plants against pathogens. Because lignin protects the cell wall polysaccharides from microbial degradation, it is also one of the most important limiting factors in the conversion of plant biomass to pulp or biofuels. The removal of lignin from the plant biomass is a difficult process.^{1,8} A glance at the structures in Scheme 1 suggests how difficult it is to extract and to process these aromatic polymers into fuels and

platform chemicals.

A promising method for converting raw biomass to usable fuel is gasification *via* pyrolysis of biomass feedstocks.^{2,9-14} Scheme 2 shows some of the common aromatics that are released in the processing of lignin.² The production of syngas ($H_2 + CO$) from biomass gasification can be used to synthesize butanol, ethanol, and other liquid fuels. The major advantage of biomass gasification *via* pyrolysis is that lignin, cellulose, and hemicellulose can all be processed. However, in the pyrolysis vapor, growth of stabilized polycyclic aromatic hydrocarbons and soot places an effective limit on the usable hydrocarbon yield of the gasification process.¹⁵

In an effort to understand and improve the biomass conversion yield, the unimolecular pyrolyses of lignin model compounds have been studied in many groups. These studies identify the initial pyrolysis intermediates, products, and mechanisms.¹⁶⁻¹⁸ There is potential to study catalysis¹⁹⁻²¹ or other means of chemical manipulation and engineering for the streamlining of biomass pyrolysis. A recent review¹ provides a "beginning-to-end" analysis of recent advances reported in the utilization of lignin.

To describe the pyrolysis and oxidation of the lignin components, several research groups have reported the pyrolysis of the simpler aromatics: phenol (C_6H_5OH),²²⁻²⁵ anisole ($C_6H_5OCH_3$),²⁶⁻³¹ and benzaldehyde (C_6H_5CHO).^{32,33} An understanding of the thermal decompositions of these singly functionalized aromatic systems has led to a predictive understanding of the more complicated

lignin model compounds such as methoxyphenol (guaiacol),³⁴⁻³⁶ dimethoxybenzene,³⁷ syringol^{38,39} and vanillin^{40,41} (see Scheme 2). In earlier studies the pyrolysis of two of the simplest molecules, phenol²⁵ and benzaldehyde,³³ were studied in a hot micro-reactor. In this paper, we explore the thermal decomposition of the *ortho* isomers of hydroxybenzaldehyde (salicylaldehyde, *o*-HOC₆H₄CHO) and dihydroxybenzene (catechol, *o*-HOC₆H₄OH). A peculiarity of salicylaldehyde and catechol is that the two substituents (-OH and -HCO) are adjacent to each other. The pyrolysis of salicylaldehyde and catechol might be more complicated than C₆H₅CHO and C₆H₅OH if the *ortho* substituents interact.

A proper set of mechanisms is ultimately required to model the pyrolysis and combustion of lignin and its components. As Pilling has succinctly stated,⁴² “chemical mechanisms must have a quantitative foundation. Mechanisms consist of explicit, coupled chemical reactions, together with rate coefficients and product yields.” Pilling’s definition of a mechanism is a tall order. Most of the aromatics in Scheme 2 are poorly characterized. We are lacking proper heats of formation, ionization energies, and decomposition rates for most of these species. To build Pilling’s mechanism for lignin pyrolysis, several steps are required. A) The separate pyrolysis pathways for the lignin components must be established. B) The branching ratios for each of the pathways must be quantified. C) Finally, the rate expressions for each of the decomposition reactions must be measured. The rate expressions in C) are needed over a wide range of temperatures and

pressures. The objective of this paper is the establishment of the initial gas-phase pyrolysis pathways for salicylaldehyde and catechol. In the following experiments, all of the decomposition products arising in the first 100 μ sec of pyrolysis are identified by the complementary detection schemes of photoionization mass spectrometry (PIMS), photoelectron photoion coincidence mass spectroscopy (PEPICO), and matrix isolation infrared absorption spectroscopy (IR).

II. Experimental

Samples of *o*-hydroxybenzaldehyde (salicylaldehyde) and *o*-dihydroxybenzene (catechol) were obtained from Sigma Aldrich with a stated purity of >99%. No further purification was performed. The catechol- d_4 ($\text{HOC}_6\text{D}_4\text{OH}$) and salicylaldehyde- d_1 ($\text{DO-C}_6\text{H}_4\text{CHO}$) were prepared by dissolving approximately 300 mg of either salicylaldehyde- d_0 (99% CDN Isotopes) in 75 mL D_2O or catechol- d_6 (99% CDN Isotopes) in 75 mL of H_2O in a separatory funnel. About 100 mL of chloroform was then added and the mixture was shaken. The organic layer containing chloroform and the extracted isotopically labeled sample were then drained from the bottom of the funnel into a round bottomed flask. The chloroform shaking process was repeated several times. The chloroform was evaporated by a roto-evaporator and the conversion yield was approximately 80%. Since both salicylaldehyde (room temperature liquid) and catechol (room temperature solid) have low vapor pressures, the molecular beams were generated by passing the carrier gas (He, Ne, or Ar) over a heated sample (30-

100°C). Dilutions were approximated by taking the ratio of the sample vapor pressure to the backing pressure of the carrier gas. Typical dilutions were about 0.1% or less.

The products of the thermal decomposition reactions were generated inside a resistively heated (300-1800 K), microtubular (0.6 – 1.0 mm ID), SiC flow reactor with either pulsed or continuous gas injection as described below. The dilute pyrolysis products generated in the reactor were expanded into vacuum ($< 10^{-6}$ Torr) and further chemistry was quenched. Multiplexed product detection and characterization was carried out with either IR spectroscopy of matrix isolated samples, (in Ne or Ar), or time-of-flight PIMS (in He or Ar).

The microtubular reactor has been described in detail.^{29,43-46} Recent computational fluid dynamics simulations⁴⁷ have found that the micro-reactors are complex, non-linear devices. Chemical reactions in the micro-reactors vary exponentially with the gas temperature (which is rising) and quadratically with the pressure (which is falling). Consequently there is a small volume (“sweet-spot”) in which most chemical reactions occur. The size and location of the sweet-spot can vary strongly with changes in the mass flow-rate, reactor dimensions (diameter, length), material (SiC, quartz, or Al₂O₃), and the nature of the buffer gas (He, Ne, Ar). In this paper four different micro-reactors have been deployed: 1 mm ID SiC reactor with pulsed He, 0.66 mm ID SiC reactor with continuous flow of He, 1 mm ID SiC reactor with pulsed Ar, and 1 mm ID SiC reactor with continuous flow of Ar.

Matrix isolation infrared spectroscopy

Roughly 200–400 Torr of carrier gas is passed over the heated sample and through a pulsed valve (30 Hz, 300 μ s open time), resulting in a cryogenic matrix deposition rate of 1-3 Torr min⁻¹. The heated microtubular reactor is separated from the cryogenic CsI collection window by a copper radiation shield with 5 mm aperture for passage of the molecular beam. The reactor output expands into the vacuum and deposits onto the CsI window (10^{-8} Torr and 4 K for Ne, or 10^{-6} Torr and 20 K for Ar). FTIR (Nicolet Magna) spectra are collected with 0.125 – 0.25 cm⁻¹ resolution and are composite averages of 1000 scans. Infrared spectroscopy is quite sensitive for the identification of dilute reaction products, and vibrational bands with IR intensities as weak as 0.1 km mol⁻¹ are readily detected.^{45,48}

Fixed frequency 118.2 nm photoionization mass spectrometry

The molecular beam is generated with a pulsed valve, in the same way as described above for matrix isolation, except that the reactor output is sent through a skimmer. However, for the fixed energy PIMS, He carrier gas is used for both its high transmission in the VUV and its high efficiency for heating. Photoionization is accomplished at 30 Hz with 118.2 nm (10.487 eV) radiation generated from the 9th harmonic of a Nd:YAG laser (Spectra Physics). This method is convenient in that the VUV generation is laser based and relatively intense.⁴⁹ A reflectron time-of-flight mass spectrometer (Jordan) with a multi-channel ion detection plate detector (MCP) is used with a mass resolution of

about 0.08 amu.

Dissociative ionization is a common problem in fixed energy PIMS detection and refers to the subsequent fragmentation of the parent ion: $AB + \hbar\omega \rightarrow [AB]^+ + e^- \rightarrow A^+ + B$. Because PIMS is used as a means to detect pyrolysis products emerging from the hot micro-reactor, dissociative ionization is a potential source of confusion. The daughter ions will obscure the parent ions characteristic of the thermal fragmentation. Dissociative ionization is commonly observed⁵⁰ in the electron impact (EI) ionization mass spectrometry of aldehydes; the resulting spectra typically contain a large peak (P-1) in addition to the parent ion peak (P). Photoionization is a more gentle ionization method than EI. The 118.2 nm PIMS of benzaldehyde³³ only contains the parent peak at m/z 106 when examined at 300 K. The $IE(C_6H_5CHO)$ is reported⁵¹ as 9.50 ± 0.08 eV and heating benzaldehyde to 1300 K shows only small signs of dissociative ionization (see Fig. 7 of ref.³³). The ionization energies for both salicylaldehyde and catechol are poorly known. The $IE(o-HOC_6H_4OH)$ was reported⁵² to be 8.6 eV while that of $o-HOC_6H_4CHO$ has not been measured. The *para* isomer has been studied⁵³ and $IE(p-HOC_6H_4CHO)$ was measured (9.32 ± 0.02 eV) by electron impact ionization; the $IE(\text{salicylaldehyde})$ is likely to be about 9.3 ± 0.1 eV. The thermochemistry and ionization energies of salicylaldehyde, catechol, and related species are collected in Table 1.

Photoionization with Tunable VUV Radiation

Synchrotrons provide intense (better than 10^{12} photons s^{-1}),

monochromated (50 meV resolution), tunable VUV radiation for molecular diagnostics. Coupled with time-of-flight mass spectrometry, this is an effective detection method. Photoionization efficiency (PIE) spectra were collected at the Advanced Light Source (ALS) Chemical Dynamics Beamline (9.0.2). PIE spectra are generated by tuning through a photon energy range, typically with 25 meV steps, and monitoring the ion counts at a particular value of m/z in the mass spectrum. This provides the identification of species based on ionization energies (IEs), and differentiation of isomers at a particular m/z based on characteristics of the PIE spectrum. The Chemical Dynamics Beamline^{54,55} and the PIMS experiment⁵⁶⁻⁵⁸ have been described in detail elsewhere. Molecular beams generated for PIMS studies at the ALS were continuous He flow for two reasons. The synchrotron light is quasi-continuous (500 MHz) and use of a continuous flow molecular beam gives signal increases of about two orders of magnitude. Equally important, the use of a continuous flow in the micro-reactor and the computational fluid dynamics is much easier to characterize.⁴⁷ A mass flow controller was used to deliver about 300 standard $\text{cm}^3 \text{min}^{-1}$ (sccm) of He through a heated sample compartment and into a 0.66 mm i.d x 2.5 cm long SiC tube. The beam was skimmed in a 2 mm aperture and expanded into the interaction region (10^{-6} Torr). The flow rate and reactor geometry were chosen based on extensive modeling and characterization. For a more complete description of the gas flow characteristics (temperature, pressure, and residence time profiles) in this reactor, see ref.⁴⁷.

The molecular beam emerging from the pyrolysis source was intersected with synchrotron VUV radiation in a pulsed electric field (17 kHz), and ions were accelerated into a field free region where they were separated by mass and detected on a time sensitive MCP detector. Typical mass spectra were composite averages of more than 10^6 sweeps of the pulsed field at each photon energy, typically with 0.05 amu mass resolution and 20-50 meV stepsize.

The pyrolysis of salicylaldehyde and catechol with photoelectron photoion coincidence (PEPICO) detection was carried out at the Swiss Light Source (SLS) VUV Beamline. The experiment at the SLS has been described in detail elsewhere,⁵⁹⁻⁶² and will be briefly summarized here. The interaction chamber is evacuated by cryopumping (roughly 5000 L s^{-1}), therefore Ar was used as the buffer gas. A backing pressure of about 750 Torr of Ar is passed over the sample and through a $100 \mu\text{m}$ pinhole, providing continuous, effusive gas injection into a 1 mm i.d. x 2.5 cm long SiC microtubular reactor. The products emerge from the reactor and are expanded into the interaction region where they are ionized in a constant electric field (120 V cm^{-1}). Photoelectrons are imaged within a few tens of ns on a position sensitive delay line anode detector and are used as time zero for time-of-flight detection of photoions in a coincidence setup.⁵⁹⁻⁶²

IV. Results and Discussion

Salicylaldehyde

Based on the decomposition pathway for phenol,²⁵ Scheme 3 shows the anticipated decomposition pathway for salicylaldehyde. The initial step in the

pyrolysis of C_6H_5OH is a keto-enol isomerization to cyclohexadienone, followed by isomerization to a bicyclo [3.1.0] ketone. The ketone fragments to carbon monoxide and cyclopentadiene (see eq. (8) in ref. ²⁵). Salicylaldehyde in Scheme 3 is asymmetric so there are two expected formyl-cyclohexadienones. Further decompositions lead to a single formyl-cyclopentadiene (C_5H_5CHO , m/z 94) followed by fragmentation to the formyl-cyclopentadienyl radical, (C_5H_4CHO , m/z 93). It is unlikely that the formyl-cyclopentadienyl radical will be stable in the hot micro-reactor and fulveneketene, $C_5H_4=C=O$ (m/z 92), is the expected product. At higher temperatures, CO loss from $C_5H_4=C=O$ leads to the unstable carbene, cyclopentadienylidene (C_5H_4 , m/z 64). The singlet carbene, C_5H_4 , is anticipated to ring open to yield the alkynes, $HC\equiv C-C\equiv C-CH_3$ and $HC\equiv C-CH_2-C\equiv CH$, or the substituted allene, $HC\equiv C-CH=C=CH_2$; all are m/z 64. Loss of H-atoms from these unsaturated alkynes will form the conjugated radicals, $HC\equiv C-C\equiv C-CH_2$ and $HC\equiv C-CH-C\equiv CH$, m/z 63.

Fig. 1 shows the 118.2 nm PIMS resulting from a dilute sample of $o\text{-HOC}_6\text{H}_4\text{CHO}$ pyrolyzed in a pulsed SiC reactor. As salicylaldehyde is heated from 300 – 1000 K in the micro-reactor, the PIMS in Fig. 1 shows only the expected parent peak at m/z 122 and the small (7 %) ^{13}C isotope peak. Even though the 118.2 nm VUV laser (10.487 eV) is roughly 1 eV above the ionization threshold for $o\text{-HOC}_6\text{H}_4\text{CHO}$ (see Table 1), there are no signals at m/z 121 characteristic of dissociative ionization. Heating $o\text{-HOC}_6\text{H}_4\text{CHO}$ to 1100 K leads to the first appearance of a signal at m/z 92 ($C_5H_4=C=O$) as suggested by

Scheme 3. Further heating of salicylaldehyde to 1200 K shows additional fragmentation to both m/z 92 and m/z 64 (predicted in Scheme 3 to be a mixture of $\text{HC}\equiv\text{C}-\text{C}\equiv\text{C}-\text{CH}_3$, $\text{HC}\equiv\text{C}-\text{CH}_2-\text{C}\equiv\text{CH}$, and $\text{HC}\equiv\text{C}-\text{CH}=\text{C}=\text{CH}_2$). The PIMS at 1300 K reveals several new species, tentatively assigned as a mixture of the C_5H_3 radicals (m/z 63), either ($\text{HC}\equiv\text{C}-\text{C}\equiv\text{C}-\text{CH}_2$, $\text{HC}\equiv\text{C}-\text{CH}-\text{C}\equiv\text{CH}$), the cyclopentadienyl radical (C_5H_5 , m/z 65), *o*-benzyne (*o*- C_6H_4 , m/z 76), and phenol ($\text{C}_6\text{H}_5\text{OH}$, m/z 94).

Fig. 2 is a scan of the 10.5 eV PIMS of salicylaldehyde pyrolyzed in a 0.66 mm ID, micro-reactor with He carrier gas at the ALS. In order to benefit from the quasi-continuous synchrotron light source, the reactor was operated continuously with the mass flow rate fixed at 280 sccm, generating the pyrolysis products in a He supersonic jet expansion. In contrast, Fig. S1 is the 10.5 eV PIMS of pyrolysis of salicylaldehyde⁶³ in a 1 mm ID micro-reactor with Ar as the carrier gas at the SLS. In this case the gas mixture is regulated by a needle valve and a continuous, effusive jet of pyrolysis products is produced. In each of these experiments, PIMS signals at m/z 92 and then m/z 64 appear early as the first pyrolysis products. Pyrolysis in a pulsed reactor (Fig. 1) and a continuous reactor (Fig. 2) yield the same results.

At higher temperatures all PIMS spectra in Figs. 1 and 2 have a fragment at m/z 94 and (1 + 1) REMPI spectra identify this as $\text{C}_6\text{H}_5\text{OH}$ (see below). In the earlier pyrolysis study³³ of $\text{C}_6\text{H}_5\text{CHO}$, the presence of H-atom chain reactions was found at higher temperatures: $\text{C}_6\text{H}_5\text{CHO} + \text{H} \rightleftharpoons [\text{C}_6\text{H}_6\text{CHO}]^* \rightarrow \text{C}_6\text{H}_6 + \text{H} +$

CO. The decomposition of fulvenketene generates the radicals ($\text{HC}\equiv\text{C}-\text{C}\equiv\text{C}-\text{CH}_2$, $\text{HC}\equiv\text{C}-\text{CH}-\text{C}\equiv\text{CH}$) and H-atoms. If the H-atoms subsequently attack the *o*- $\text{HOC}_6\text{H}_4\text{CHO}$ sample, two decomposition pathways become possible as shown in Scheme 4. Addition of H-atoms to the phenyl ring yields an activated complex, $[\text{HOC}_6\text{H}_6\text{CHO}]^*$, which can collapse to phenol and the formyl radical (top of Scheme 4). Because the CH bond energy⁶⁴ of HCO is only 16 kcal mol^{-1} , the formyl radicals will never survive in the hot micro-reactor. Dissociation of HCO to CO and H-atoms ensues and the H-atoms continue the chain reaction.

Instead of adding to the phenyl ring, the H-atoms could attack the carbonyl group of salicylaldehyde in two different manners; see the bottom of Scheme 4. The most stable adduct results from addition to the oxygen to form the hydroxybenzyl radical: $o\text{-HOC}_6\text{H}_4\text{CHO} + \text{H} \rightleftharpoons [o\text{-HOC}_6\text{H}_4\text{CHOH}]^*$. This benzyl radical persists before reverting back to H-atoms and salicylaldehyde. In contrast, H-atom addition to produce the alkoxy radical, $[o\text{-HOC}_6\text{H}_4\text{-CH}_2\text{-O}]^*$, triggers several fragmentations. From the earlier case of benzaldehyde,³³ one anticipates that the $o\text{-HOC}_6\text{H}_4\text{-CH}_2\text{-O}$ radical will fragment to $\text{CH}_2=\text{O}$ and the *o*-hydroxy-phenyl radical, $o\text{-HOC}_6\text{H}_4$. Hydroxy-phenyl radicals have been scrutinized earlier⁶⁵ and it was found that they easily rearrange to the phenoxy radical: $o\text{-HOC}_6\text{H}_4 \rightarrow \text{C}_6\text{H}_5\text{O}$. Phenoxy radicals decarbonylate^{27,29,65} to cyclopentadienyl radicals, C_5H_5 (*m/z* 65), that further fragment to $\text{HC}\equiv\text{CH}$ and HCCCH_2 . Instead of isomerizing to phenoxy, the $o\text{-HOC}_6\text{H}_4$ radical could lose OH

to produce *o*-benzyne, $o\text{-C}_6\text{H}_4$ (m/z 76). It is known⁶⁶ that benzyne decomposes to $\text{HC}\equiv\text{C}-\text{C}\equiv\text{CH} + \text{HC}\equiv\text{CH}$.

At the highest reactor temperatures, all PIMS have salicylaldehyde pyrolysis products at m/z 76 (benzyne), 65 (cyclopentadienyl radical), 50 (diacetylene), and 39 (propargyl radical). The presence of both $\text{CH}_2=\text{O}$ and $\text{HC}\equiv\text{CH}$ (from $o\text{-C}_6\text{H}_4$ fragmentation) are detected by IR spectroscopy (see below). At first glance, it seems as if Schemes 3 and 4 properly describe the pyrolysis of $o\text{-HOC}_6\text{H}_4\text{CHO}$.

As stated in the introduction, an interesting feature of salicylaldehyde is the *ortho* relationship of the $-\text{OH}$ and $-\text{CHO}$ groups. Because $m\text{-HOC}_6\text{H}_4\text{CHO}$ is an isomer of salicylaldehyde, Fig. 3 is the control experiment. Salicylaldehyde and its two isomers have similar thermodynamic properties (see Table 1). The keto-enol fragmentation pathway outlined for salicylaldehyde in Scheme 1 will equally apply to both of the isomeric $m\text{-HOC}_6\text{H}_4\text{CHO}$ and $p\text{-HOC}_6\text{H}_4\text{CHO}$. A glance at the thermal cracking of $m\text{-HOC}_6\text{H}_4\text{CHO}$ in Fig. 3 shows that there is a problem with the keto-enol chemistry in Scheme 3. Instead of pyrolysis of $m\text{-HOC}_6\text{H}_4\text{CHO}$ beginning about 1100 K to produce a single species, m/z 92, the decomposition of $m\text{-HOC}_6\text{H}_4\text{CHO}$ produces fragments at m/z 94 (phenol), m/z 66 (cyclopentadiene), m/z 65 (cyclopentadienyl radical) and m/z 39 (propargyl radical) at 1300 K. The feature at m/z 94 is positively identified to be $\text{C}_6\text{H}_5\text{OH}$ by its (1 + 1) REMPI spectrum (Fig. 3) recorded at NREL.⁴⁰ At 1400 K, a new feature at m/z 78 grows in. This is certainly benzene. But there are no m/z 92

signals present in Fig. 3. Comparison of the PIMS spectra in Figs. 1 and 3 implies that the keto-enol pathway in Scheme 3 is not a low-energy path for salicylaldehyde decomposition. There must be another pathway for pyrolysis of *o*-HOC₆H₄CHO (m/z 122) to produce fulvenketene (m/z 92).

Catechol

Catechol has recently been subjected to catalytic pyrolysis with a zeolite catalyst, identifying fulvenone ketene using the PEPICO technique at the SLS.⁶⁷ Earlier studies have subjected *o*-HOC₆H₄OH to pyrolysis in tubular reactors with residence times of a few seconds. The decomposition products were collected and were analyzed by gas chromatography (GC) with EI mass spectroscopy⁶⁸ or flame ionization detection.⁶⁹ Instead of GC analysis products have been trapped in on the cold finger of a Dewar mounted inside an EPR cavity.^{70,71} EPR spectroscopy was then used to identify the product radicals. A set of DFT/RRKM calculations⁷² have been used to interpret these results. Preliminary results for the pyrolysis of catechol and hydroquinone with a heated SiC micro-reactor have been presented.²⁵

To anticipate the results of pyrolysis of *o*-HOC₆H₄OH, Scheme 5 applies the keto-enol chemistry²⁵ of phenol to catechol, *o*-HOC₆H₄OH (m/z 110). This predicts the loss of CO to generate the hydroxyl-cyclopentadiene, HOC₅H₅ (m/z 82). The C-H bond energy of the parent cyclopentadiene⁷³ is 83 kcal mol⁻¹; consequently we expect that loss of H from hydroxyl-cyclopentadiene to generate the hydroxyl-cyclopentadienyl radical (m/z 81) will require about 80 kcal mol⁻¹.

Further decomposition of the C_5H_4OH radical leads to H-atom and to the well characterized^{48,74-77} cyclopentadienone, $C_5H_4=O$ (m/z 80).

Fig. 5 is the 118.2 nm PIMS that is observed when a sample of catechol is heated in a pulsed, 1 mm SiC micro-reactor. The 400 K spectrum shows the expected parent peak at m/z 110; there is no dissociative ionization observed at 10.487 eV (See Table 1). At 1300 K, features in the PIMS appear at m/z 82 and 92. Based on Scheme 5, m/z 82 is assigned as hydroxyl-cyclopentadiene but m/z 92 does not appear in this scheme. In the spectra of salicylaldehyde (Figs 1-2), the major product was m/z 92 and was assigned as fulveneketene. Like salicylaldehyde, it seems that o - HOC_6H_4OH is also cracking to $C_5H_4=C=O$. The catechol spectrum in Fig. 5 agree with earlier findings.^{25,40} Fig. 5 shows that heating catechol to 1500 K produces several new products at m/z 94 (phenol), m/z 80 ($C_5H_4=O$), m/z 78 (C_6H_6), m/z 76 (o - C_6H_4), m/z 65 (C_5H_5), m/z 64 (possible mixture of $HC\equiv C-C\equiv C-CH_3$, $HC\equiv C-CH_2-C\equiv CH$, $HC\equiv C-CH=C=CH_2$), m/z 63 (either $HC\equiv C-C\equiv C-CH_2$ or $HC\equiv C-CH-C\equiv CH$), m/z 54 ($CH_2=CH-CH=CH_2$), m/z 52 ($CH_2=CH-C\equiv CH_2$), m/z 50 ($HC\equiv C-C\equiv CH$), and m/z 39 ($HCCCH_2$). Separate (1 + 1) REMPI spectra⁴⁰ confirm the identity of the m/z 94 feature as phenol.

The pyrolysis of catechol- d_4 is consistent with that of catechol- d_0 . Pyrolysis of o - HOC_6D_4OH (m/z 114) in Fig. 6 produces hydroxyl-cyclopentadiene- d_4 (m/z 86) and cyclopentadienone- d_4 (m/z 84). Decomposition of $C_5D_4=O$ generates acetylene- d_2 and $DC\equiv C-CD=CD_2$ (m/z 58). However, just as in the case of catechol- d_0 , fulveneketene- d_4 (m/z 96) is formed. Thermal cracking of $C_5D_4=C=O$

(*m/z* 96) produces a mixture of [$\text{CD}_3\text{C}\equiv\text{C}-\text{C}\equiv\text{CD}$, $\text{HC}\equiv\text{C}-\text{CD}_2-\text{C}\equiv\text{CD}$, and $\text{HC}\equiv\text{C}-\text{CD}=\text{C}=\text{CD}_2$] (*m/z* 68) as well as D atoms and the radicals at *m/z* 66 ($\text{CD}_2\text{C}\equiv\text{C}-\text{C}\equiv\text{CD}$ and $\text{HC}\equiv\text{C}-\text{CD}-\text{C}\equiv\text{CD}$).

As discussed earlier for salicylaldehyde, the keto-enol pathway for catechol (Scheme 5) should equally apply to resorcinol or hydroquinone. Resorcinol is *m*-HO-C₆H₄-OH and is an isomer of *o*-HO-C₆H₄-OH. Fig. 7 is the PIMS of the pyrolysis of resorcinol and is presented as a control the thermal cracking of catechol. Catechol begins decomposition at 1300 K (Fig. 5) but *m*-HO-C₆H₄-OH starts fragmenting at 1400 K to *m/z* 66 (C₅H₆) and small amounts of *m/z* 81 (probably HC≡C-CHC(O)CH₃) and *m/z* 82 (likely HC≡C-CH₂C(O)CH₃). No signals at *m/z* 92 are ever observed for resorcinol. A detailed analysis of the pyrolysis of *m*-HO-C₆H₄-OH in Fig. 7 is beyond the scope of this paper.

Schemes 5 for the decomposition of catechol is now suspect because it does not have a pathway to generate fulveneketene-d₀ (*m/z* 92) or fulveneketene-d₄ (*m/z* 96). It does not seem that the keto-enol chemistry²⁵ of phenol describes a low energy decomposition pathway for catechol.

How could the thermal cracking of *o*-HOC₆H₄OH produce the C₅H₄=C=O (*m/z* 92) in Figs. 5 and 6? A possible connection of the pyrolysis of catechol to that of salicylaldehyde is shown in Scheme 6. Loss of H₂O from catechol (*m/z* 110) could produce the keto-carbene at *m/z* 92; subsequent rearrangement of this carbene leads to fulveneketene. If catechol-d₄ is the substrate, C₅D₄=C=O (*m/z* 96), would be predicted. Scheme 6 also shows a pathway for pyrolysis of

salicylaldehyde (m/z 122) to result in loss of H_2 with the production of a reactive ketene, m/z 120. Loss of CO from the m/z 120 ketene, generates the same, m/z 92 keto-carbene which isomerizes to the observed fulveneketene, m/z 92. Notice that H_2 pathway for salicylaldehyde in Scheme 6 is distinct from the keto-enol route in Scheme 3.

The predictions of Scheme 6 offering a path to fulveneketene can be tested by infrared spectroscopy. The matrix IR spectra that result from heating either o - HOC_6H_4OH (black trace) or o - HOC_6H_4CHO (red scan) to 1300 K in a pulsed, Ar micro-reactor are shown in Fig. 8. The green spectrum is that of the Ar carrier gas heated to 1300 K. The IR spectra of Fig. 8 show the presence of known modes of $C_5H_4=C=O$ (ν_3 , ν_5 , ν_7 , and ν_{26}) resulting from the pyrolysis of either catechol or salicylaldehyde. Characteristic bands for methyl-diacetylene, ν_1 and $\nu_{11}(HC\equiv C-C\equiv C-CH_3)$, acetylene, $\nu_3(HC\equiv CH)$, and propargyl radical, $\nu_1(HCCCH_2)$, are detected in Fig. 9. The IR spectra in Fig. 10 identify cyclopentadienone as a thermal decomposition product of catechol; the known⁴⁸ bands (ν_3 , ν_{14} , ν_{15} , ν_{21}) of $C_5H_4=O$ are all clearly present. The IR spectra of Figs. 8 – 10 as well as the PIMS in Figs. 1, 2, 5, and 6 demonstrate that both $C_5H_4=C=O$ and $HC\equiv C-C\equiv C-CH_3$ result from the pyrolysis of either o - HOC_6H_4OH or o - HOC_6H_4CHO .

Fig. 11 is further confirmation of the H-atom/salicylaldehyde chain reactions at the bottom of Scheme 4. The IR spectra in Fig. 11 demonstrate that pyrolysis of o - HOC_6H_4CHO produces $HC\equiv CH$ and $CH_2=O$. The 11.5 eV PIMS in

the bottom right hand panel also confirms the presence of HC≡CH (m/z 26) and CH₂=O (m/z 30).

Because of the differences between the PIMS of *o*-HOC₆H₄CHO and *m*-HOC₆H₄CHO in Figs. 1 and 3, an alternative scheme for pyrolysis of salicylaldehyde was proposed at the top of Scheme 6. The detection of molecular hydrogen would be a “signature” for Scheme 6. Unfortunately the 118.2 nm PIMS cannot ionize H₂ (see Table 1) and homonuclear diatomic molecules do not absorb in the IR. Fig. 12 shows the results of a search with a synchrotron for H₂ following the pyrolysis of *o*-HOC₆H₄CHO. Figure 12 is a set of PIMS scans of a mixture of (salicylaldehyde-d₀ and salicylaldehyde-d₁) that were recorded by the synchrotron at the ALS. Heating (*o*-HOC₆H₄CHO and *o*-DO-C₆H₄CHO) to 1100 K leads to the production of both H₂ (m/z 2) and HD (m/z 3). The spectra in the left panel of Fig. 12 show that the synchrotron VUV energy of 15.5 eV is sufficient to ionize both H₂ and HD (see Table 1). Scheme 6 also provides an explanation for the feature at m/z 120 in the PIMS recorded by synchrotron at the SLS (Fig. S1). Entraining salicylaldehyde in Ar with a continuous 1 mm micro-reactor leads to an effusive beam of the dissociation products. At reactor temperatures of 900, 1000, and 1100 K, there is clearly a pyrolysis product at m/z 120. Scheme 6 assigns this product as the ketene, O=C₆H₄=C=O.

The PIMS spectra of H₂ and HD in Fig. 12 show only the smallest traces of H-atoms. It is straightforward to show⁷⁵ that the photoion signal, J⁺(H atom), is proportional to the density of H-atoms (n_H) and the photoionization cross section,

$\sigma(\text{H})$. The photoionization cross sections for H-atom⁷⁸ and molecular⁷⁹ H_2 have been reported. At the photoionization energy of Fig. 12, $\sigma(\text{H}, 15.5 \text{ eV}) = 4.7 \times 10^{-18} \text{ cm}^2$ while $\sigma(\text{H}_2, 15.5 \text{ eV}) = 1.3 \times 10^{-18} \text{ cm}^2$. So the ratio of ion signals at 15.5 eV in Fig. 12 can be written:

$$\frac{J^+(\text{H-atom})}{J^+(\text{H}_2)} \cong \frac{n_{\text{H}} \sigma(\text{H-atom})}{n_{\text{H}_2} \sigma(\text{H}_2)} = \frac{4n_{\text{H}}}{n_{\text{H}_2}} \quad (1)$$

The observed $J^+(\text{H-atom})$ signals in Fig. 12 are small compared to either $J^+(\text{H}_2)$ or $J^+(\text{HD})$ so we conclude that there are very few H-atoms in the beam relative to H_2 or HD.

V. Conclusion

The pyrolysis of (salicylaldehyde, catechol) is a complicated process. It is clear that for both species, the lowest decomposition pathways feature the interaction of the two *ortho*-substituents as described in Scheme 6. Pyrolysis of salicylaldehyde in Figs. 1 and 2 leads to initial production of fulveneketene (m/z 92) about 1100 K. Heating salicylaldehyde⁸⁰ to 1200 K continues decomposition to fulveneketene and subsequent fragmentation of $\text{C}_5\text{H}_4=\text{C}=\text{O}$ to the ($\text{HC}\equiv\text{C}-\text{C}\equiv\text{C}-\text{CH}_3$, $\text{HC}\equiv\text{C}-\text{CH}_2-\text{C}\equiv\text{CH}$, $\text{HC}\equiv\text{C}-\text{CH}=\text{C}=\text{CH}_2$) mixture at m/z 64. By 1300 K this mixture of alkynes releases H-atoms and the set of radicals ($\text{HC}\equiv\text{C}-\text{C}\equiv\text{C}-\text{CH}_2$, $\text{HC}\equiv\text{C}-\text{CH}-\text{C}\equiv\text{CH}$,) at m/z 63. The H-atom chemistry, as outlined in Scheme 4, produces $\text{CH}_2=\text{O}$ (m/z 30), $\text{C}_6\text{H}_5\text{OH}$ (m/z 94), *o*-benzyne (m/z 76). Further fragmentation of phenol generates cyclopentadiene (m/z 66) that leads to C_5H_5 (m/z 65). The cyclopentadienyl radicals further fragment to

$\text{HC}\equiv\text{CH}$ (m/z 26) and HCCCH_2 (m/z 39). The keto-enol chemistry outlined in Scheme 3 is consistent with all of PIMS and IR spectra of salicylaldehyde pyrolysis products. But Scheme 3 can be applied to (*m*- $\text{HOC}_6\text{H}_4\text{CHO}$ and *p*- $\text{HOC}_6\text{H}_4\text{CHO}$) where it fails. Consequently we are forced to Scheme 6 that is confirmed by the PIMS detection of (H_2 and HD) as decomposition products from the (*o*- $\text{HOC}_6\text{H}_4\text{CHO}$, *o*- $\text{DOC}_6\text{H}_4\text{CHO}$) mixture.

The pyrolysis of catechol is even more complex. Heating *o*- $\text{HOC}_6\text{H}_4\text{OH}$ to 1300 K produces both hydroxyl-cyclohexadiene (m/z 82) and fulvenketene (m/z 92). It seems that both the catechol fragmentations in Scheme 5 and Scheme 6 are operational here. As the pyrolysis temperature is raised to 1500 K, the $\text{C}_5\text{H}_4=\text{C}=\text{O}$ decomposes to the C_5H_4 alkynes (m/z 64) and H-atoms plus the C_5H_3 mixture of radicals (m/z 63). The H-atoms attack the starting catechol to produce phenol (m/z 94). Phenol further decomposes to CO and cyclopentadiene (m/z 66) that rapidly fragments to C_5H_5 (m/z 65) and on to HCCH (m/z 26) plus HCCCH_2 (m/z 39). There is a minor fragmentation pathway for $\text{C}_6\text{H}_5\text{OH}$ (see Figs. 1 and 7 in ref.²⁵) that leads to (*o*-benzyne, H_2O); this is the source of diacetylene (m/z 50). The hydroxyl-cyclopentadiene (m/z 82) decomposes to $\text{C}_5\text{H}_4=\text{O}$ (m/z 80) that produces⁷⁵ $\text{HC}\equiv\text{C}-\text{CH}=\text{CH}_2$ (m/z 52) and $\text{HC}\equiv\text{CH}$.

The decomposition of salicylaldehyde to H_2 and $[\text{O}=\text{C}_6\text{H}_4=\text{C}=\text{O}] \rightarrow \text{CO} + \text{C}_5\text{H}_4=\text{C}=\text{O}$ (Scheme 6) is a striking result. We believe that the formation of H_2 is a concerted process rather than the result of step-wise H atom abstractions. We have already invoked H-atom chain reactions as being responsible for the

generation of $\text{CH}_2=\text{O}$, benzyne, and $\text{C}_6\text{H}_5\text{OH}$ (Figs 1, 2, and 11). But the 15.5 eV PIMS in Fig. 12 demonstrate that density of H-atoms is much less than that of molecular hydrogen (H_2 and HD). As far as we know there have been no kinetic studies of $\text{H} + \text{HOC}_6\text{H}_4\text{CHO} \rightarrow \text{products}$. Reactions of H-atoms with $\text{C}_6\text{H}_5\text{CHO}$ have been investigated⁸¹ but the H-atoms always add to the aromatic ring and never lead to formation of H_2 . Reactions of phenol with H-atoms⁸² was observed to produce H_2 and $\text{C}_6\text{H}_5\text{O}$. For the case of salicylaldehyde, such an H-atom abstraction would generate the $\text{OC}_6\text{H}_4\text{-CHO}$ radical. It is known³⁴ that phenoxy radicals easily lose CO to form cyclopentadienyl radicals; consequently one anticipates that the $\text{OC}_6\text{H}_4\text{-CHO}$ radicals would produce formyl cyclopentadienyl radicals, $\text{C}_5\text{H}_4\text{-CHO}$ (m/z 93). Scheme 3 predicts that $\text{C}_5\text{H}_4\text{-CHO}$ will decompose to fulveneketene, $\text{C}_5\text{H}_4=\text{C}=\text{O}$ (m/z 92) — which is observed. Such H-atom abstractions for *m*- $\text{HOC}_6\text{H}_4\text{CHO}$ and *o*- $\text{HOC}_6\text{H}_4\text{CHO}$ would predict formation of $\text{C}_5\text{H}_4=\text{C}=\text{O}$ (m/z 92) for these isomers but this is not observed. However because only trace amounts of H-atoms are observed in the PIMS of Fig. 12, we believe that most of the observed H_2 is the result of electrocyclic processes in Scheme 6.

The only other report⁸³ of H_2 formation by a concerted elimination is that of the pyrolysis of 1,4-cyclohexadiene at (500 K — 900 K) to hydrogen and benzene. Gas chromatographic detection of benzene was accomplished but the loss of H_2 had to be inferred. A reviewer has made the point that “significant amounts of H_2 from the pyrolysis of the salicylaldehyde, could trigger a phenomenon called dihydrogen catalysis.⁸⁴ Dihydrogen assisted

dehydrogenation of salicylaldehyde could form the m/z 120-product, similar to what occurs with tetralin and other compounds interacting with H_2 which significantly lowers the activation energy.” The concerted loss of H_2 is an interesting process and warrants further detailed examination.

Early theoretical studies⁷⁰⁻⁷² of the pyrolysis of catechol predicted a concerted elimination of water to a singlet carbene. This is described in Scheme 6 and accounts for the formation of the observed fulveneketene, $C_5H_4=C=O$ (m/z 92) from catechol but not resorcinol.

We return to the lignin structure itself in Scheme 1. Do these findings of the pyrolysis pathways for o - HOC_6H_4CHO and o - HOC_6H_4OH , or those of the lignin components in Scheme 2, provide any insight to the pyrolysis of lignin itself? We believe so. The weak bonds in Scheme 1 are the aryl ether linkages. Because of the aromatic stabilization of the phenoxy radical, the bond energy for anisole, $C_6H_5O-CH_3$, is 63 kcal mol^{-1} (see footnote 63 in ref.³⁴). There are a large number of $O-CH_3$ bonds in all lignins. As the structure in Scheme 1 is heated, most of the peripheral $-C_6H_4O-CH_3$ bonds will rupture over a narrow temperature range to release CH_3 radicals.³⁷ At slightly lower temperatures the aryl ether linkages along the backbone of the lignin in Scheme 1 will disintegrate; such a breakage is shown in Scheme 7. Cleavage along the backbone at the dotted line (top of Scheme 7) will require roughly 60 kcal mol^{-1} and generates a (phenoxy, alkyl) radical pair. The resulting alkyl radical (bottom of Scheme 7) is subject to β -scission to produce H-atom and a substituted styrene. The sister phenoxy radical

has two pathways. As observed earlier,^{27,29,34,37} phenoxy radicals decarbonylate rapidly to release cyclopentadienyl radicals that fragment to substituted cyclopentadienones⁷⁵ and CH₃ radicals. A more interesting fate of the phenoxy radicals is that they may suffer a Mulcahy rearrangement^{37,85-88} to produce salicylaldehyde derivatives and H-atoms. The salicylaldehydes follow the pathway of Scheme 6 to substituted fulvenketenes and more H-atoms.

These conjectures predict that heating lignin samples to a threshold temperature will release a shower of CO, H-atoms and CH₃ radicals. The radicals, particularly the H-atoms, trigger chain reactions³³ (see Scheme 4) that will trigger the wholesale destruction of the aromatic lignin polymer.

VI. Acknowledgements

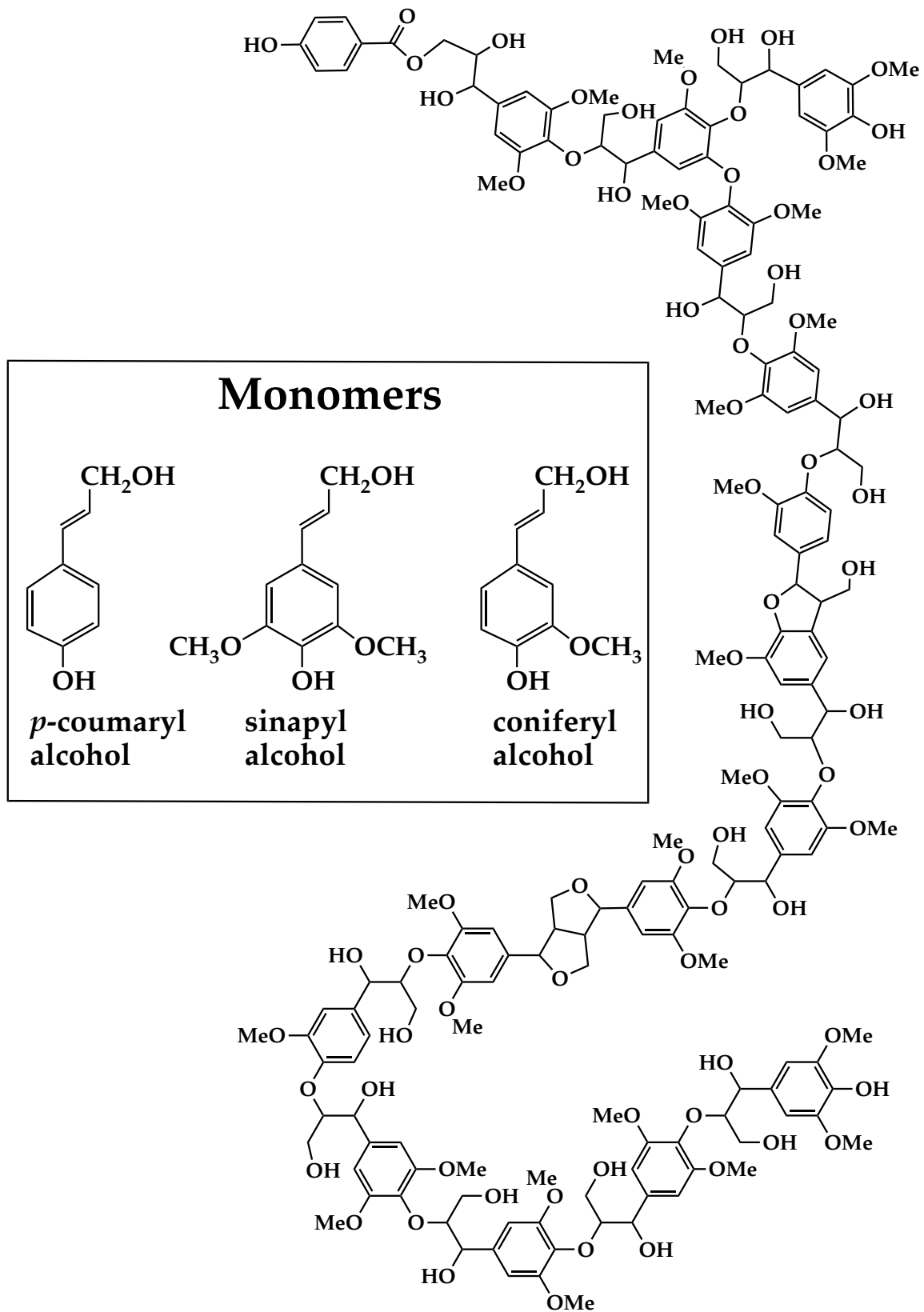
We would like to acknowledge support from U.S. National Science Foundation (CHE-1112466) for TKO, GBE, and JWD. M.A., T.P.T and the experiments at the chemical dynamics beamline at the ALS were supported by the Director, Office of Science, Office of Basic Energy Sciences, of the US Department of Energy under contract no. DE-AC02-05CH11231, through the Gas Phase Chemical Physics Program, Chemical Sciences Division. MRN and DJR are supported by United States Department of Energy's Bioenergy Technology Office, under Contract No. DE-AC36-99GO10337 with the Sciences Division of the U.S. Department of Energy under Contract No. DE-AC02-05CH11231. Some of the experiments were carried out at the VUV beamline of the Swiss Light Source located at the

Paul Scherrer Institute, Villigen Switzerland. PH was supported by the Swiss Federal Office for Energy (BFE Contract Number SI/501269-01). Finally we note that for many decades our work has benefited from the leadership and companionship of Prof. Dr. Hanna Reisler and we thank her.

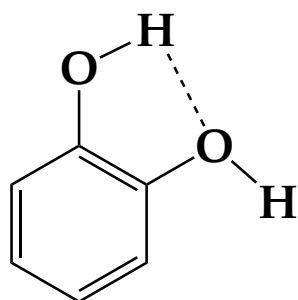
Table 1. Thermochemistry

	$\Delta_f H_{298} / \text{kJ mol}^{-1}$	$\Delta_f H_{298} / \text{kcal mol}^{-1}$	
$\text{C}_6\text{H}_5\text{OH}$ (phenol)	-96.4 ± 0.9	-23.0 ± 0.2	89
<i>o</i> -HO-C ₆ H ₄ -OH (catechol)	-267.5 ± 1.9	-63.9 ± 0.5	90
<i>m</i> -HO-C ₆ H ₄ -OH (resorcinol)	-274.7 ± 2.2	-65.7 ± 0.5	89
<i>p</i> -HO-C ₆ H ₄ -OH (hydroquinone)	-265.3 ± 2.3	-63.4 ± 0.5	89
<i>o</i> -HO-C ₆ H ₄ -CHO (salicylaldehyde)	-245.6 ± 2.2	-58.7 ± 0.5	91
<i>m</i> -HO-C ₆ H ₄ -CHO	-213.7 ± 0.6	-51.1 ± 0.1	92
<i>p</i> -HO-C ₆ H ₄ -CHO	-217.8 ± 0.4	-52.1 ± 0.1	92
<hr/>			
$D_0(\text{C}_6\text{H}_5\text{O-H})$	$3.721 \pm 0.004 \text{ eV}$	$85.8 \pm 0.1 \text{ kcal mol}^{-1}$	93
$D_0(o\text{-HOC}_6\text{H}_4\text{O-H})$	$\leq 3.407 \pm 0.006 \text{ eV}$	$78.6 \pm 0.1 \text{ kcal mol}^{-1}$	94
<hr/>			
$IE(\text{H})$	$13.59843449402 \pm 0.00000000001 \text{ eV}$		95
$IE(\text{H}_2)$	$15.42580277 \pm 0.0000005 \text{ eV}$		95
$IE(\text{HD})$	$15.44452374 \pm 0.0000004 \text{ eV}$		96
$IE(\text{C}_6\text{H}_5\text{OH})$	$8.508 \pm 0.001 \text{ eV}$		97
$IE(o\text{-HO-C}_6\text{H}_4\text{-OH})$	$8.6 \pm 0.1 \text{ eV}$		52
$IE(m\text{-HO-C}_6\text{H}_4\text{-OH})$	$8.6 \pm 0.1 \text{ eV}$		52
$IE(p\text{-HO-C}_6\text{H}_4\text{-OH})$	$8.4 \pm 0.1 \text{ eV}$		52
$IE(o\text{-HO-C}_6\text{H}_4\text{-CHO})$	—		
$IE(m\text{-HO-C}_6\text{H}_4\text{-CHO})$	—		
$IE(p\text{-HO-C}_6\text{H}_4\text{-CHO})$	$9.32 \pm 0.02 \text{ eV}$		53
$IE(\text{HC}\equiv\text{CH})$	$11.4006 \pm 0.0002 \text{ eV}$		98
$IE(\text{CH}_2=\text{O})$	$10.8850 \pm 0.0002 \text{ eV}$		99

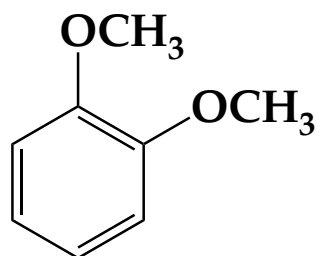
$EA(C_6H_5O)$	2.2538	± 0.0008	eV	100
$EA(o-HOC_6H_4O)$	2.3292	± 0.0004	eV	101,102
$EA(m-HOC_6H_4O)$	2.3292	± 0.0004	eV	103



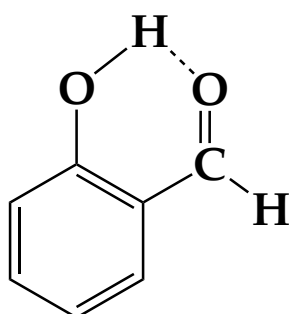
Scheme 1. Partial lignin structure from poplar trees; adapted from Vanholme *et al.*⁸



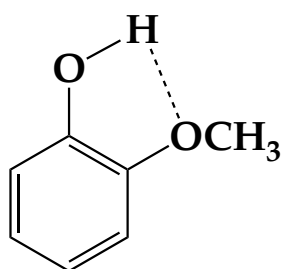
catechol^{25,40}



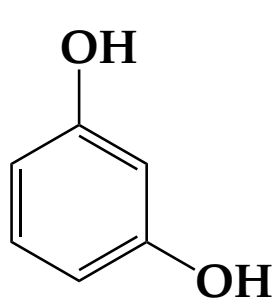
o-dimethoxy
-benzene³⁷



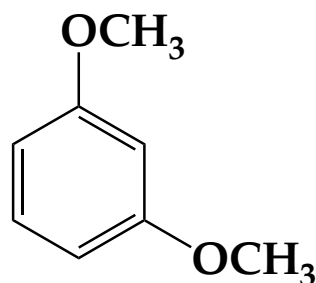
salicylaldehyde³⁷



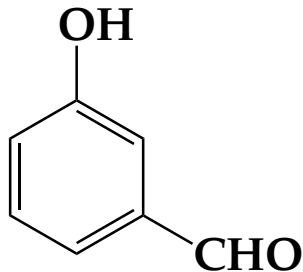
o-guaiacol³⁴⁻³⁶



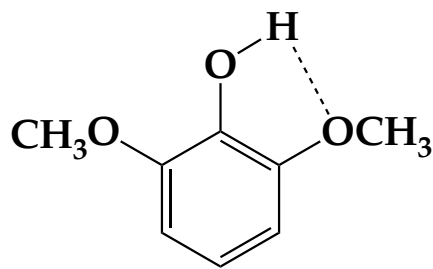
resorcinol⁴⁰



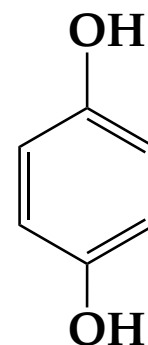
m-dimethoxy
-benzene³⁷



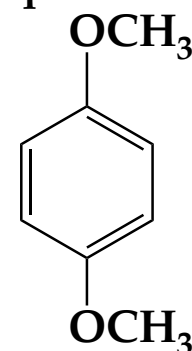
3-hydroxy-
benzaldehyde³⁷



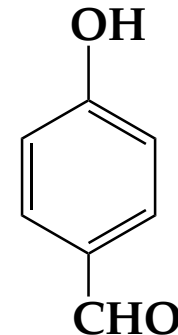
syringol^{38,39}



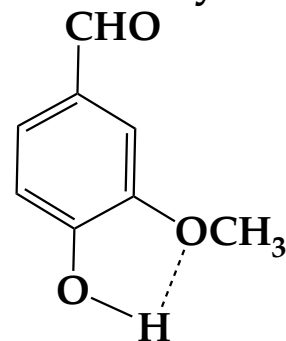
hydroquinone⁴⁰



p-dimethoxy
-benzene³⁷

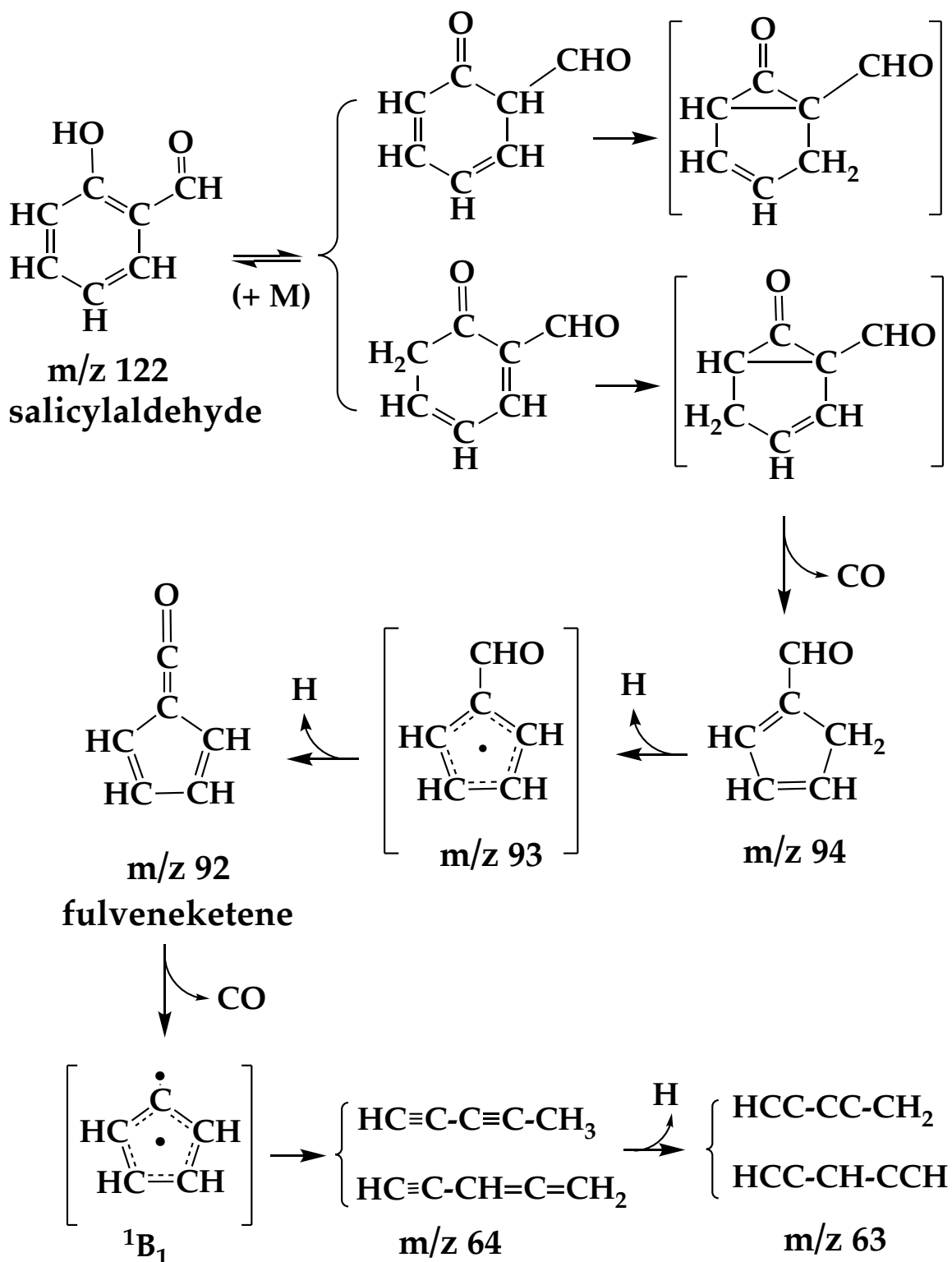


4-hydroxy-
benzaldehyde³⁷

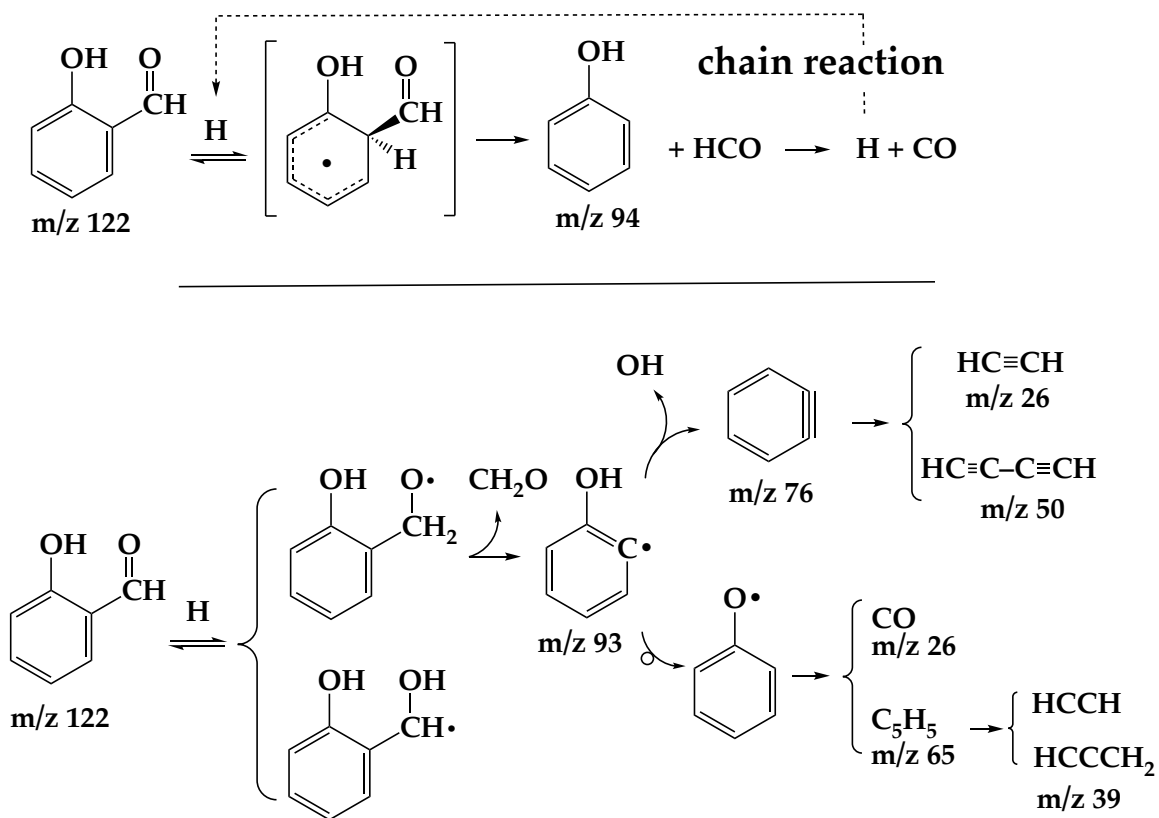


vanillin^{40,41}

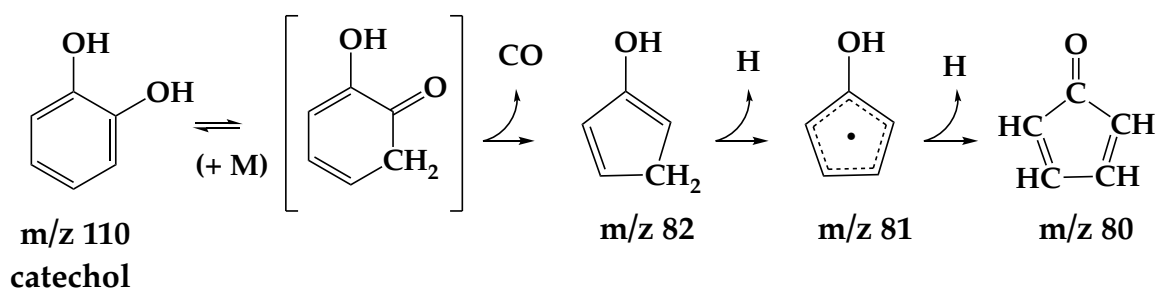
Scheme 2. Some common components associated with lignins.



Scheme 3. Application of the phenolic keto-enol tautomerism pathway²⁵ to the thermal decomposition of salicylaldehyde.

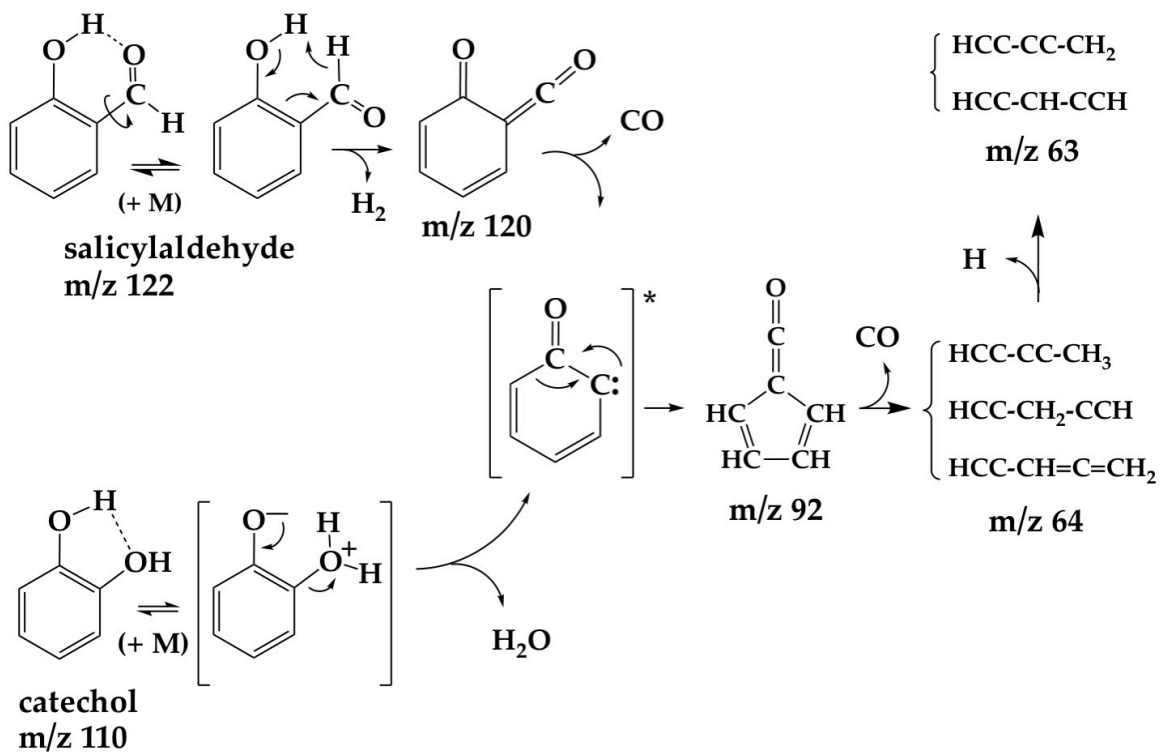


Scheme 4. Possible H-atom chain reactions³³ in the thermal decomposition of salicylaldehyde.

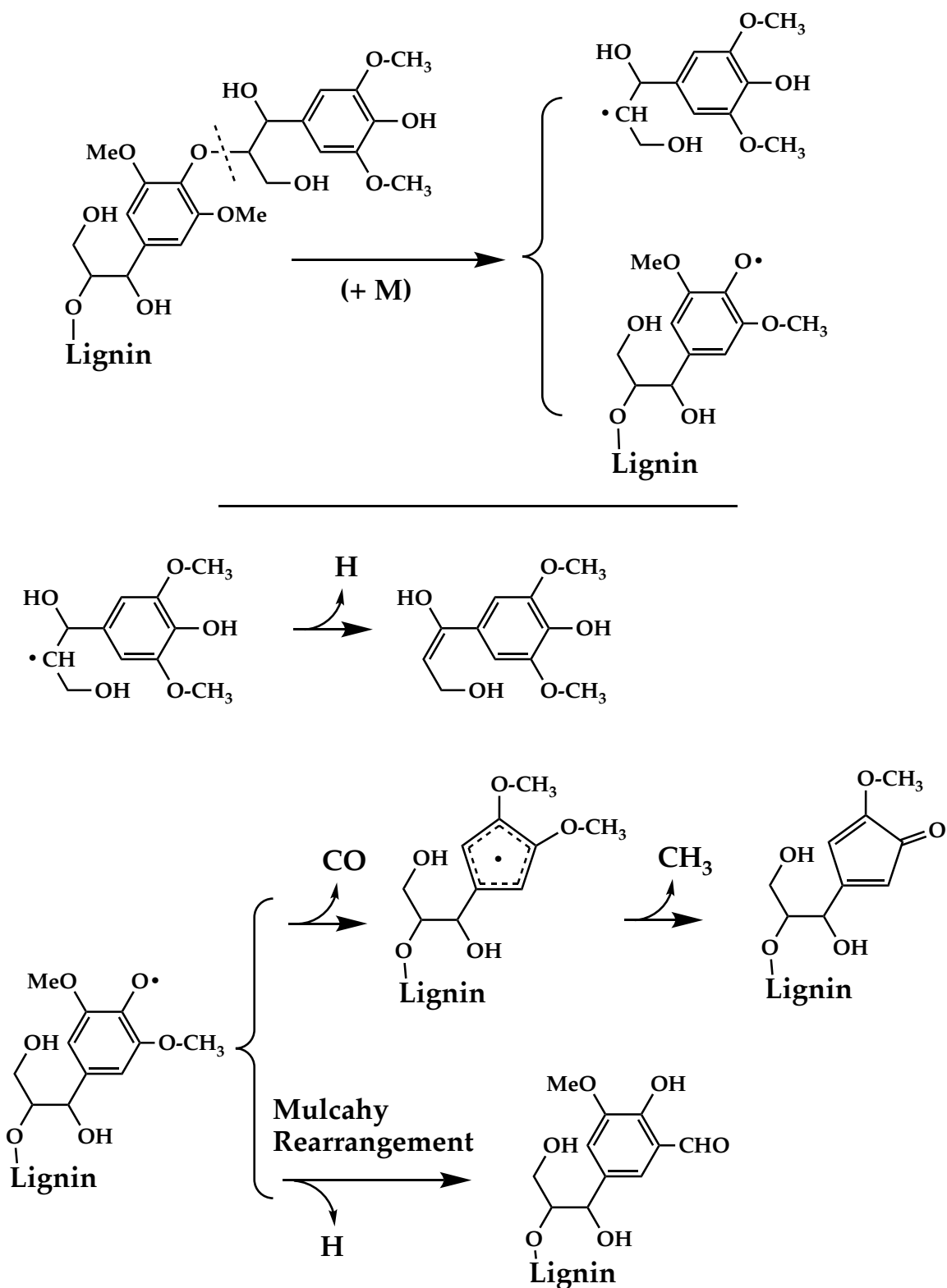


Scheme 5. Application of the phenolic keto-enol tautomerism²⁵ in the thermal decomposition of catechol.

Pyrolysis Pathways for Salicylaldehyde and Catechol



Scheme 6. Interaction of the functional groups in the thermal decomposition of both salicylaldehyde and catechol are predicted to generate fulveneketene, m/z 92.



Scheme 7. The initial steps conjectured for the pyrolysis of lignin in Scheme 1.

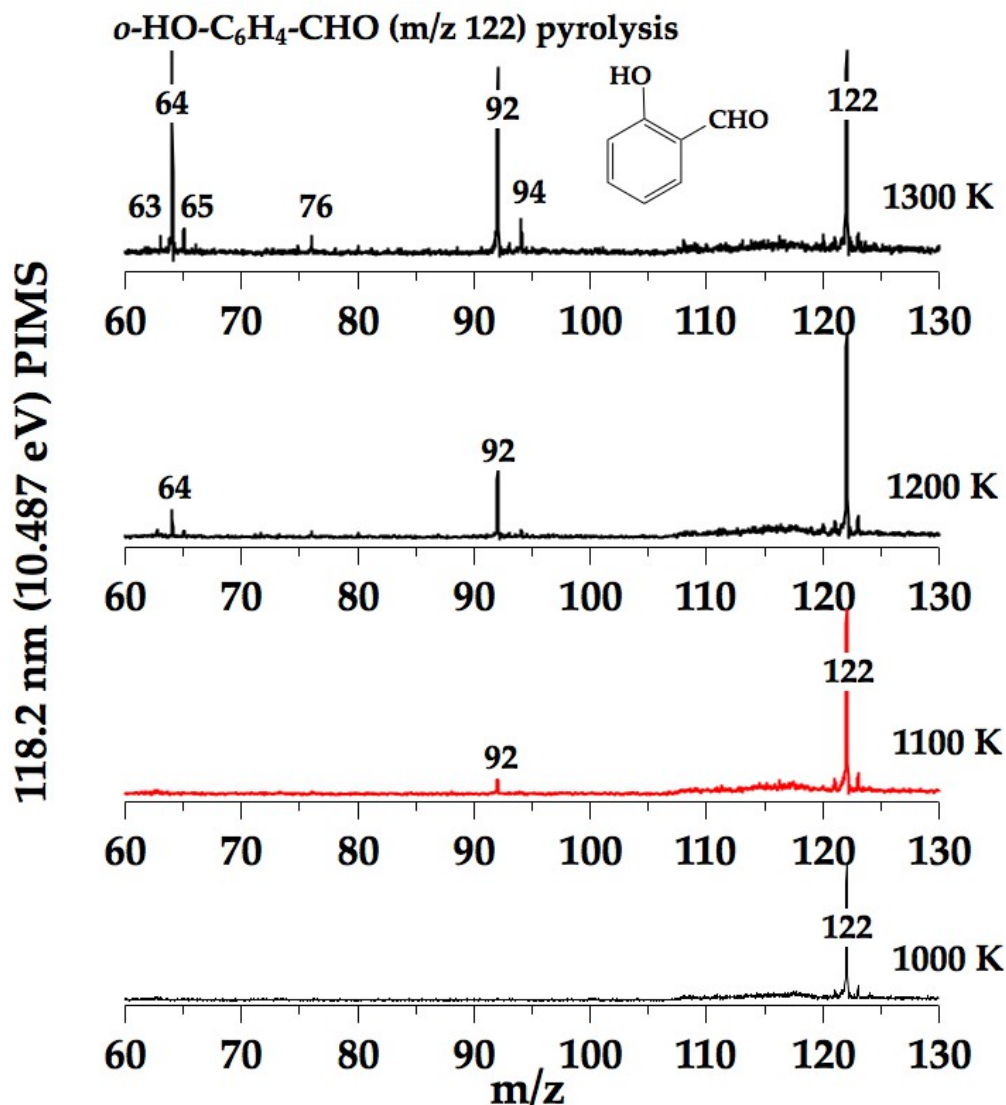


Fig. 1. The 118.2 nm (10.487 eV) spectrum of salicylaldehyde diluted (0.1 % or less) in He and pulsed through a 1 mm ID SiC reactor. The onset of pyrolysis identifies first m/z 92 (C₅H₄=C=O) and then 64 (HC≡C-C≡C-CH₃, HC≡CCH₂C≡CH, HC≡C-CH=C=CH₂) as the initial thermal decomposition products. Further heating generates signals at m/z 63 (HC≡C-C≡C-CH₂ or HC≡C-CH-C≡CH), m/z 65 (C₅H₅), m/z 76 (*o*-C₆H₄) and m/z 94 (C₆H₅OH).

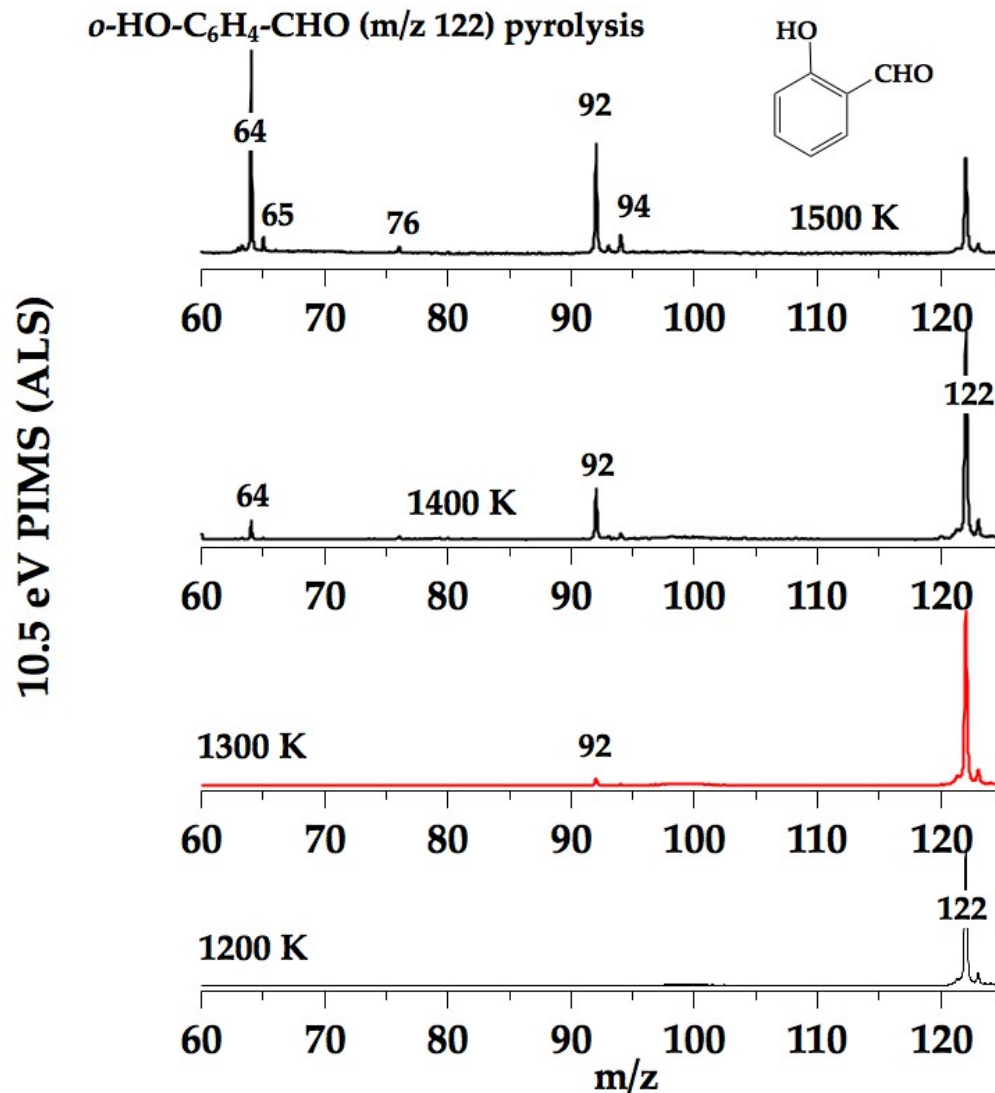


Fig. 2. The ALS synchrotron VUV (10.5 eV) PIMS spectra of salicylaldehyde diluted (0.1 % or less) in He with continuous flow through a 0.66 mm ID reactor. The initial thermal decomposition product at m/z 92 is C₅H₄=C=O at 1300 K, followed by m/z 64 (HC≡C-C≡C-CH₃, HC≡CCH₂C≡CH, HC≡C-CH=C=CH₂) at 1400 K. Further heating generates products at m/z 65 (C₅H₅) 76 (*o*-C₆H₄), and 94 (C₆H₅OH).

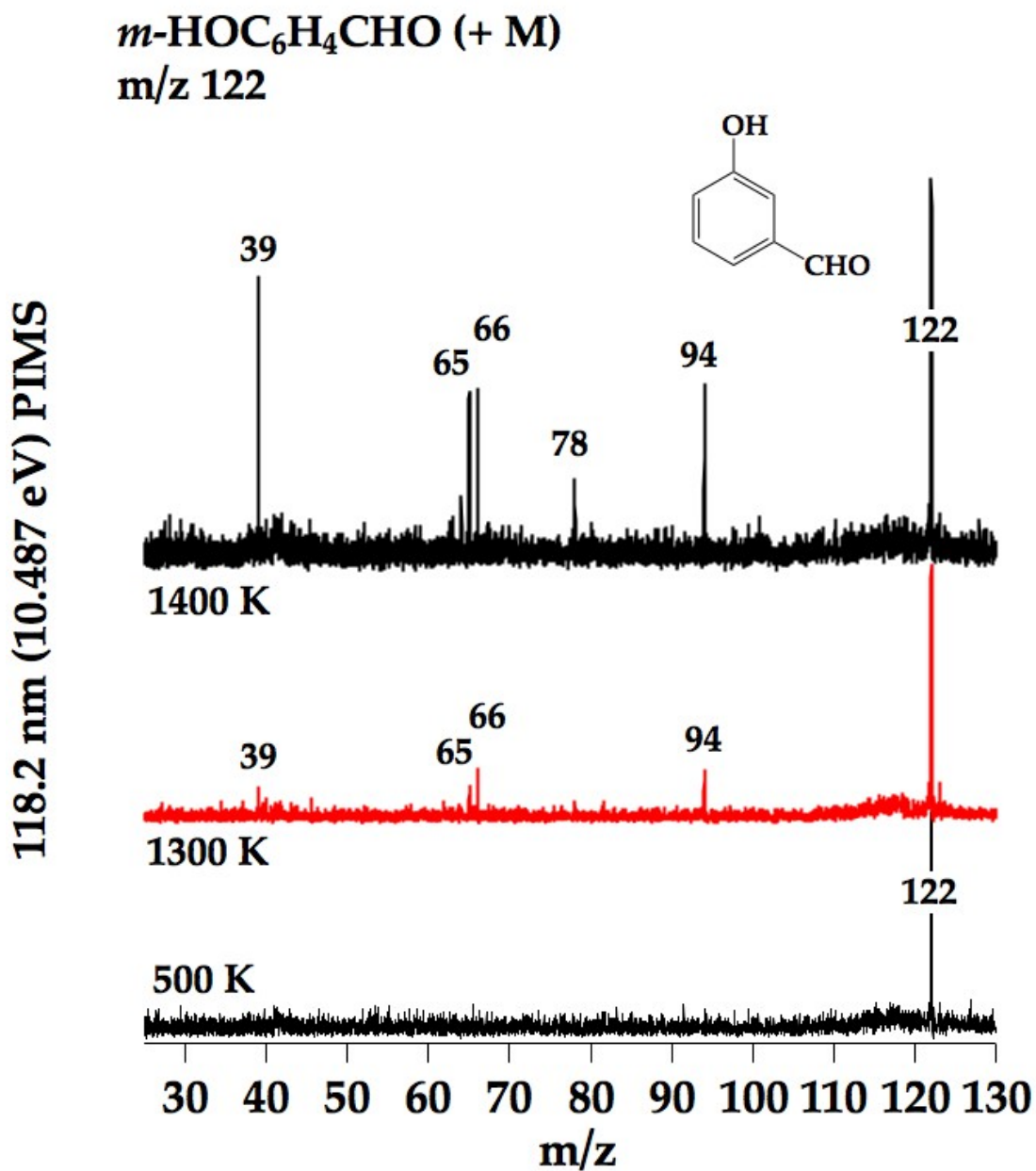


Fig. 3. The 118.2 nm (10.487 eV) PIMS resulting from heating a mixture of roughly 1 Torr *m*-hydroxybenzaldehyde in 2000 Torr He (0.05%) in a pulsed, 1 mm ID SiC reactor. The onset of pyrolysis identifies first m/z 94 (C₅H₅OH), 66 (C₅H₆), and m/z 39 (HCCCH₂) as the initial thermal decomposition products. No signals at m/z 92 (C₅H₄=C=O) are found.

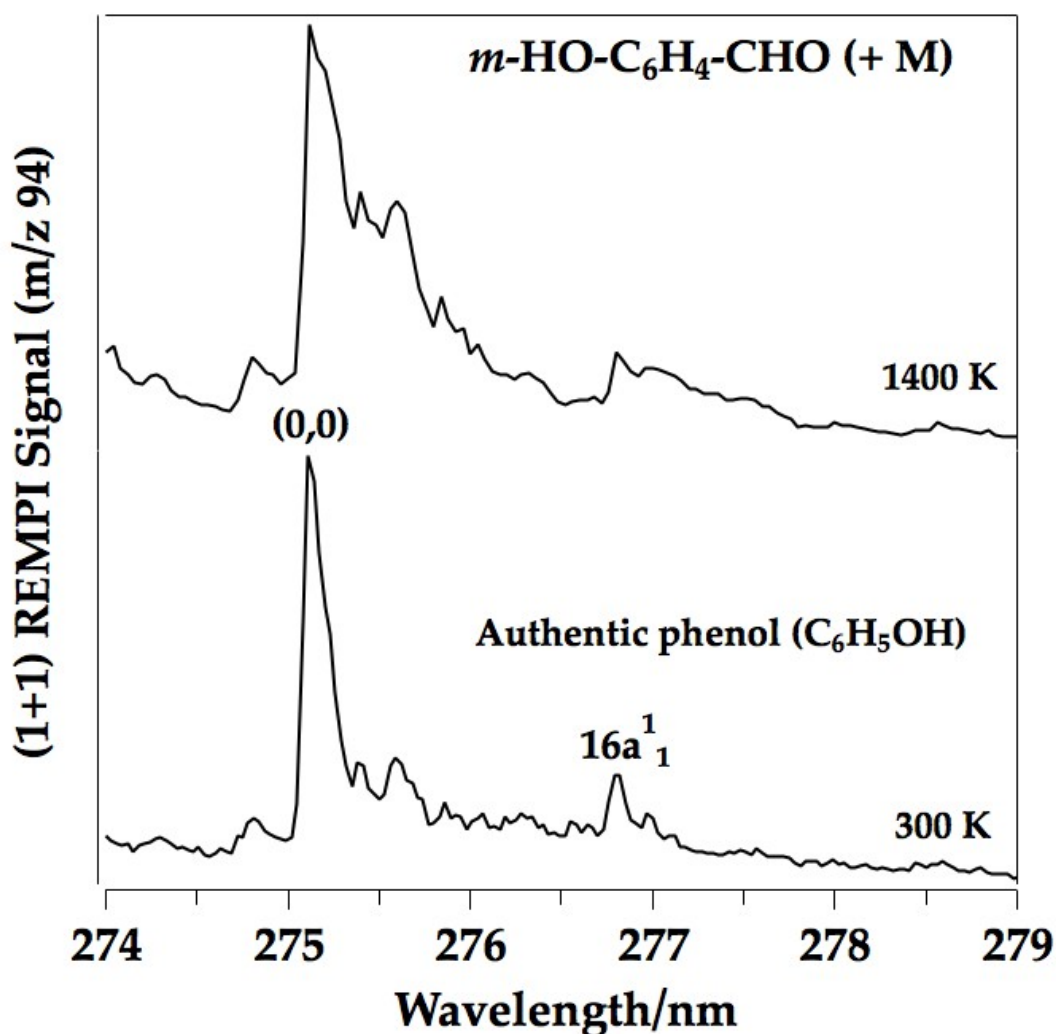


Fig. 4 The resonance-enhanced multiphoton ionization (REMPI) spectrum of the cracking products of *meta*-hydroxybenzaldehyde. The top trace is a REMPI scan of the pyrolysis of *m*-HO-C₆H₄-CHO at 1400 K. These spectra record the presence of the C₆H₆OH⁺ ion at *m/z* 94 resulting from a (1 + 1) REMPI process. The laser scanned over the known¹⁰⁴⁻¹⁰⁶ phenol resonance, $\tilde{A}^1A'' (^1B_2) \leftarrow \tilde{X}^1A' (^1A_1)$, corresponding to $T_0(\text{C}_6\text{H}_5\text{OH}) = 275.1 \text{ nm}$ or 36348.9 cm^{-1} (4.507 eV). The $IE(\text{C}_6\text{H}_5\text{OH})$ is reported⁹⁷ to be $8.508 \pm 0.001 \text{ eV}$ so absorption of a 2nd 275 nm photon leads to ionization. The top trace is a 0.3 to 0.4% *m*-HO-C₆H₄-CHO/He mixture heated in the pulsed reactor to 1400 K. The bottom trace is an authentic sample of phenol and expanded

through the micro-tubular reactor at room temperature. The (0,0) transition for C_6H_5OH is observed at 275.1 nm. Figs 1 and 2 show small amounts of phenol (m/z 94) at the high temperature pyrolysis of salicylaldehyde. The (1 + 1) REMPI (similar to Fig. 3) verify that this m/z 94 feature is C_6H_5OH .

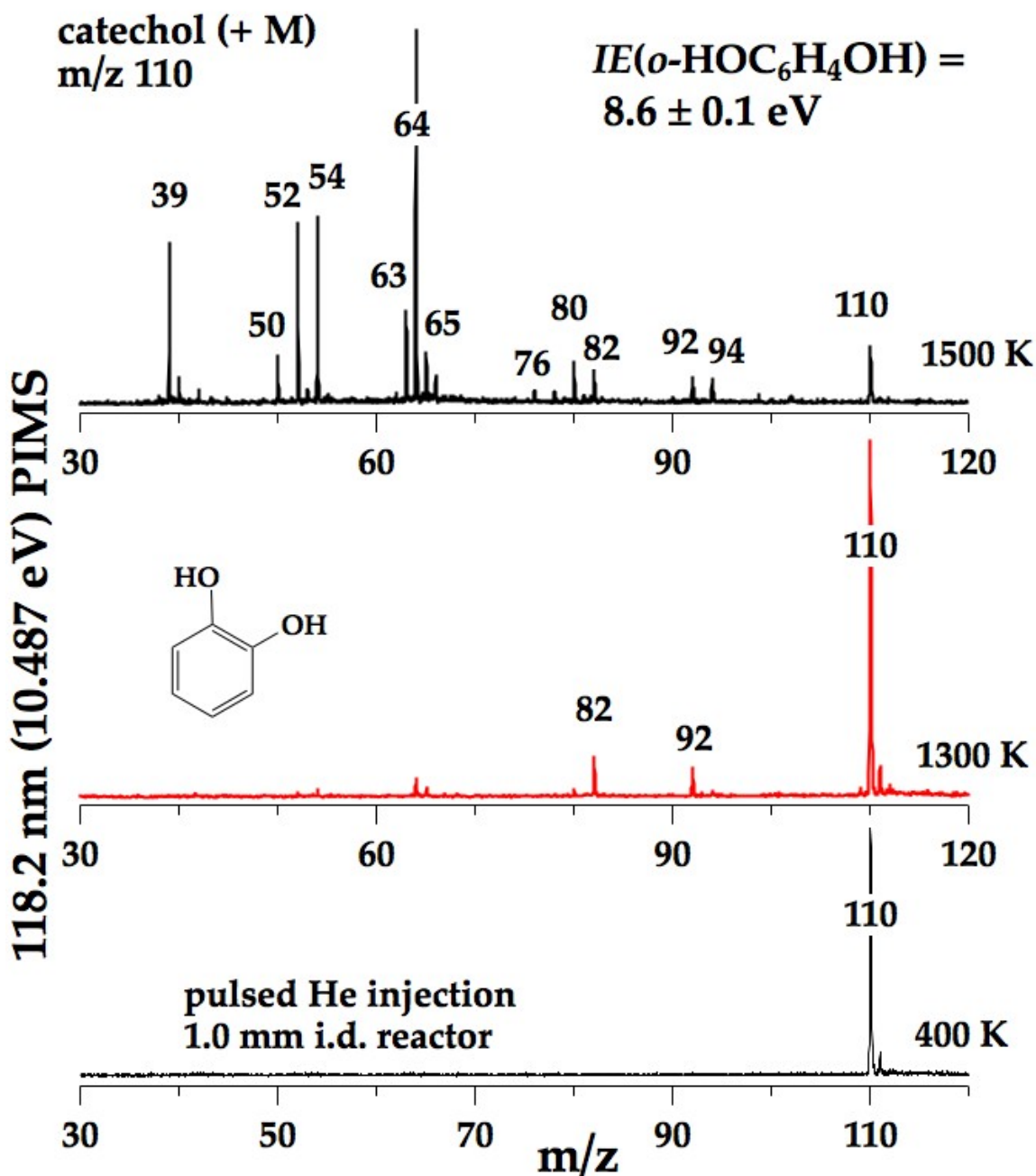


Fig. 5. The thermal decomposition of catechol (m/z 110) diluted in He pulsed into a 1 mm ID SiC reactor shows m/z 82 ($\text{C}_5\text{H}_5\text{OH}$) and m/z 92 ($\text{C}_5\text{H}_4=\text{C}=\text{O}$) as the initial decomposition products. Further heating generates products at m/z 39 (HCCCH_2), m/z 50 ($\text{HC}\equiv\text{C}-\text{C}\equiv\text{CH}$), m/z 52 ($\text{HC}\equiv\text{C}-\text{CH}=\text{CH}_2$), m/z 54 ($\text{CH}_2=\text{CH}-\text{CH}=\text{CH}_2$), m/z 63 ($\text{HCC}-\text{CC}-\text{CH}_2$ or $\text{HCC}-\text{CH}-\text{CCH}$), m/z 64

($\text{HC}\equiv\text{C}-\text{C}\equiv\text{C}-\text{CH}_3$, $\text{HC}\equiv\text{C}-\text{CH}_2-\text{C}\equiv\text{C}-\text{CH}_3$, or $\text{HC}\equiv\text{C}-\text{CH}=\text{C}=\text{CH}_2$), m/z 65 (C_5H_5),
and m/z 80 ($\text{C}_5\text{H}_4=\text{O}$).

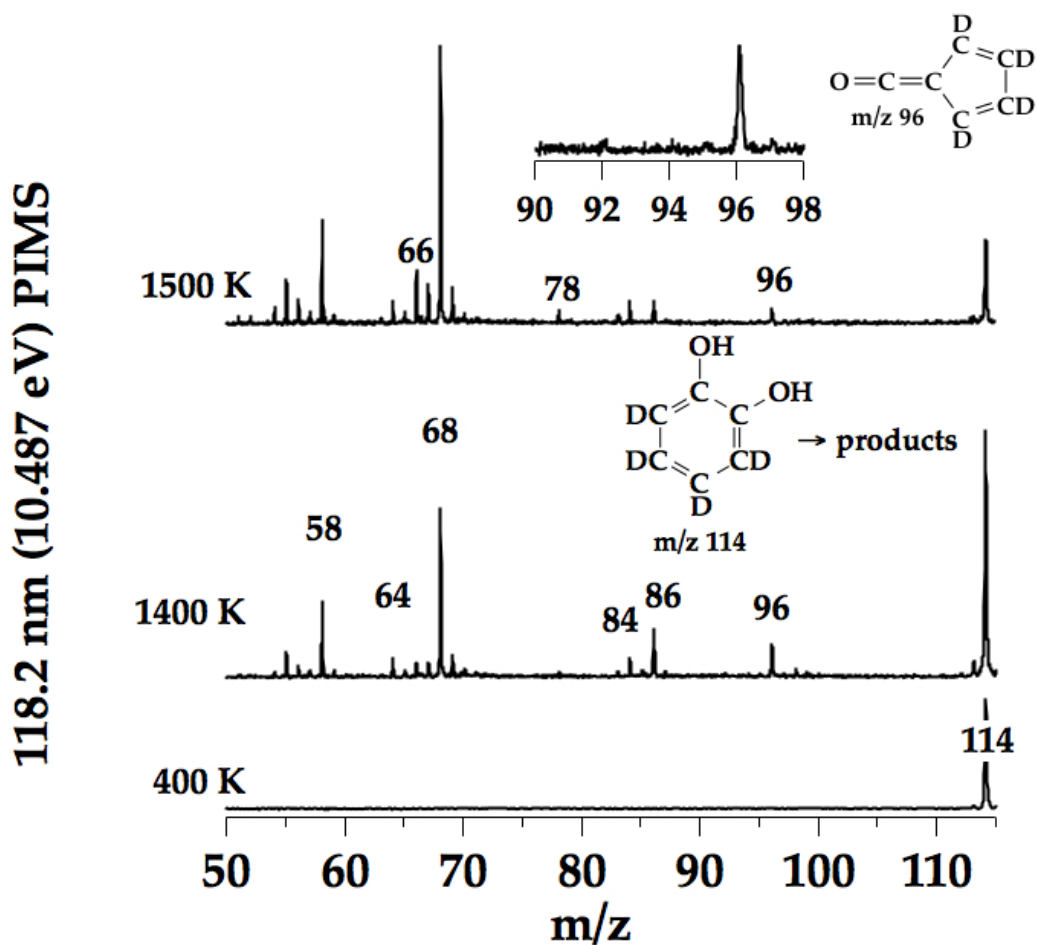


Fig. 6. The thermal decomposition of catechol- d_4 (m/z 114) diluted in He and pulsed into a 1 mm ID SiC reactor. Assignments are m/z 96 ($C_5D_4=O$), m/z 68 ($DC\equiv C-C\equiv CCD_3$, $DC\equiv C-CD_2-C\equiv CCD$ or $DC\equiv C-CD=C=CD_2$), m/z 66 ($DC\equiv C-C\equiv CCD_2$ or $DC\equiv C-CD-C\equiv CD$); m/z 58 is not easily assigned.

resorcinol (+ M)

$IE(m\text{-HOC}_6\text{H}_4\text{OH}) = 8.6 \pm 0.1 \text{ eV}$

m/z 110

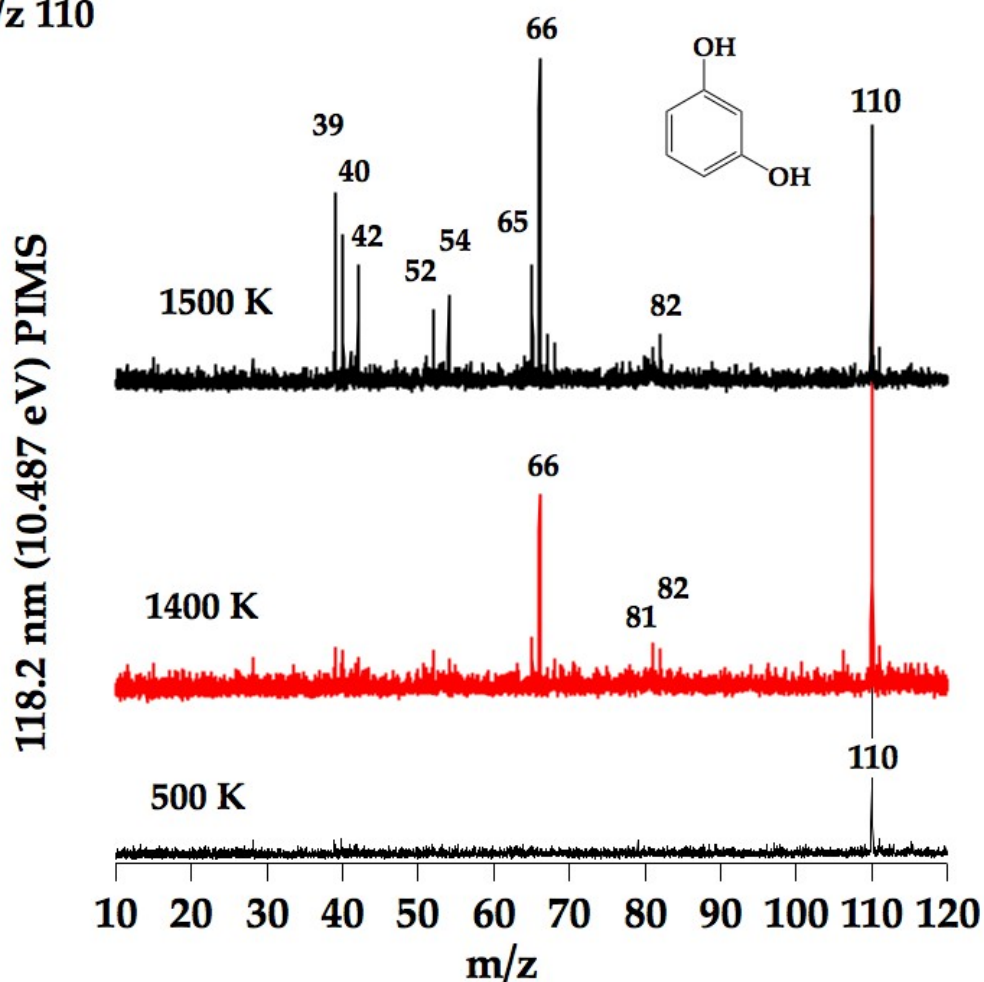


Fig. 7. The 118.2 nm (10.487 eV) PIMS resulting from heating a mixture of approximately 1 Torr resorcinol (an isomer of catechol) in 2000 Torr He (0.05%) in a pulsed, 1 mm ID SiC reactor. The onset of pyrolysis of $m\text{-HOC}_6\text{H}_4\text{OH}$ at 1400 K identifies only products at m/z 66 (C_5H_6). No signals at m/z 92 ($\text{C}_5\text{H}_4=\text{C}=\text{O}$) are observed.

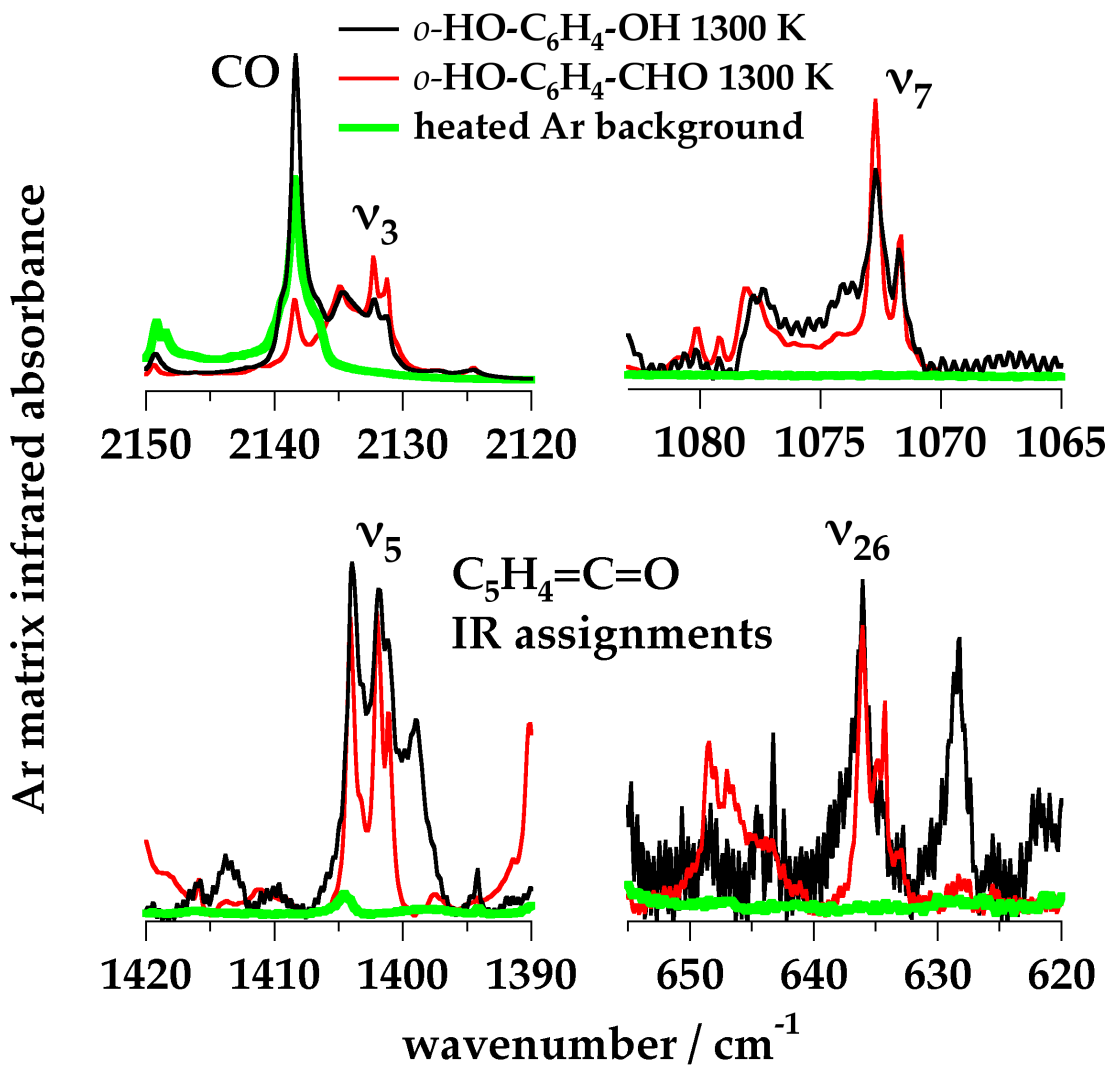


Fig. 8. The pulsed Ar matrix isolation IR spectrum of the thermal decomposition products of both salicylaldehyde and catechol show identical peaks in good agreement with IR bands arising from $\text{C}_5\text{H}_4=\text{C}=\text{O}$.

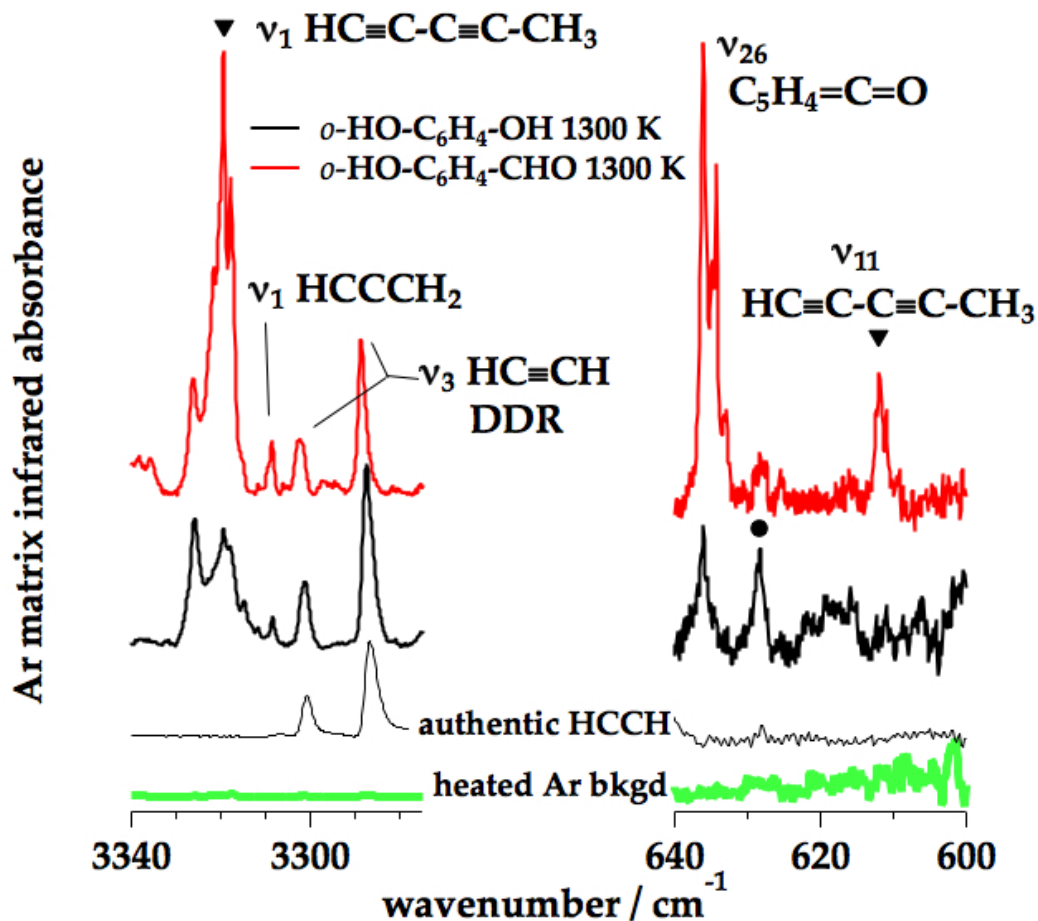


Fig. 9. The Ar matrix isolation IR spectrum of the thermal decomposition products of both salicylaldehyde and catechol show identical peaks arising from the vibrations of methyl diacetylene ($\text{HC}\equiv\text{C}-\text{C}\equiv\text{CCH}_3$), propargyl radical (HCCCH_2), fulveneketene ($\text{C}_5\text{H}_4=\text{C}=\text{O}$), and acetylene (HCCH). The bullet in the right panel is a known⁴⁸ vibration (ν_{15}) of $\text{C}_5\text{H}_4=\text{O}$ generated from the thermal decomposition of catechol.

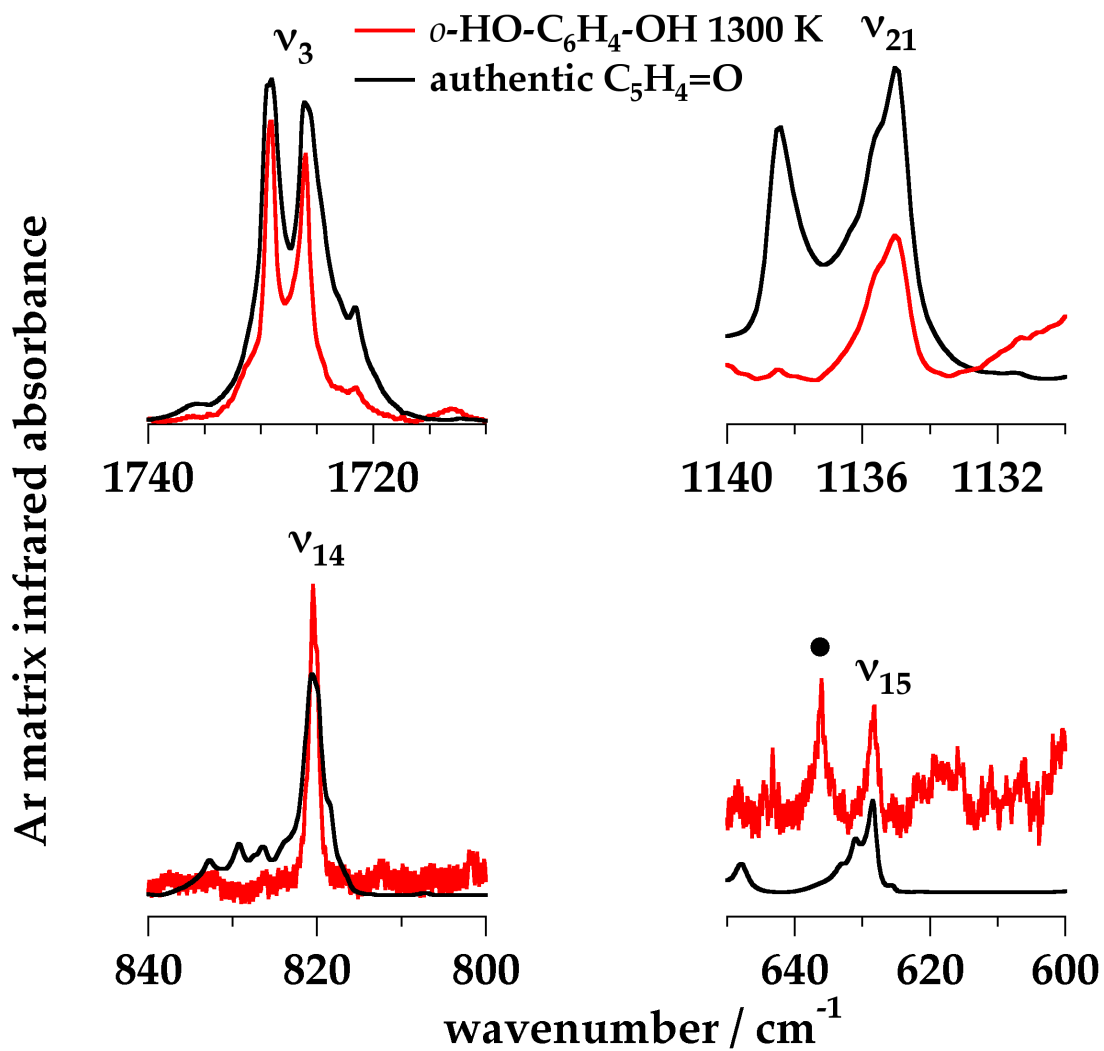


Fig. 10. The Ar matrix isolation IR spectrum of the thermal decomposition products of catechol have includes the known⁴⁸ IR bands (ν_3 , ν_{14} , ν_{15} , ν_{21}) of $\text{C}_5\text{H}_4=\text{O}$. The bullet (\bullet) marks $\nu_{26}(\text{C}_5\text{H}_4=\text{C}=\text{O})$.

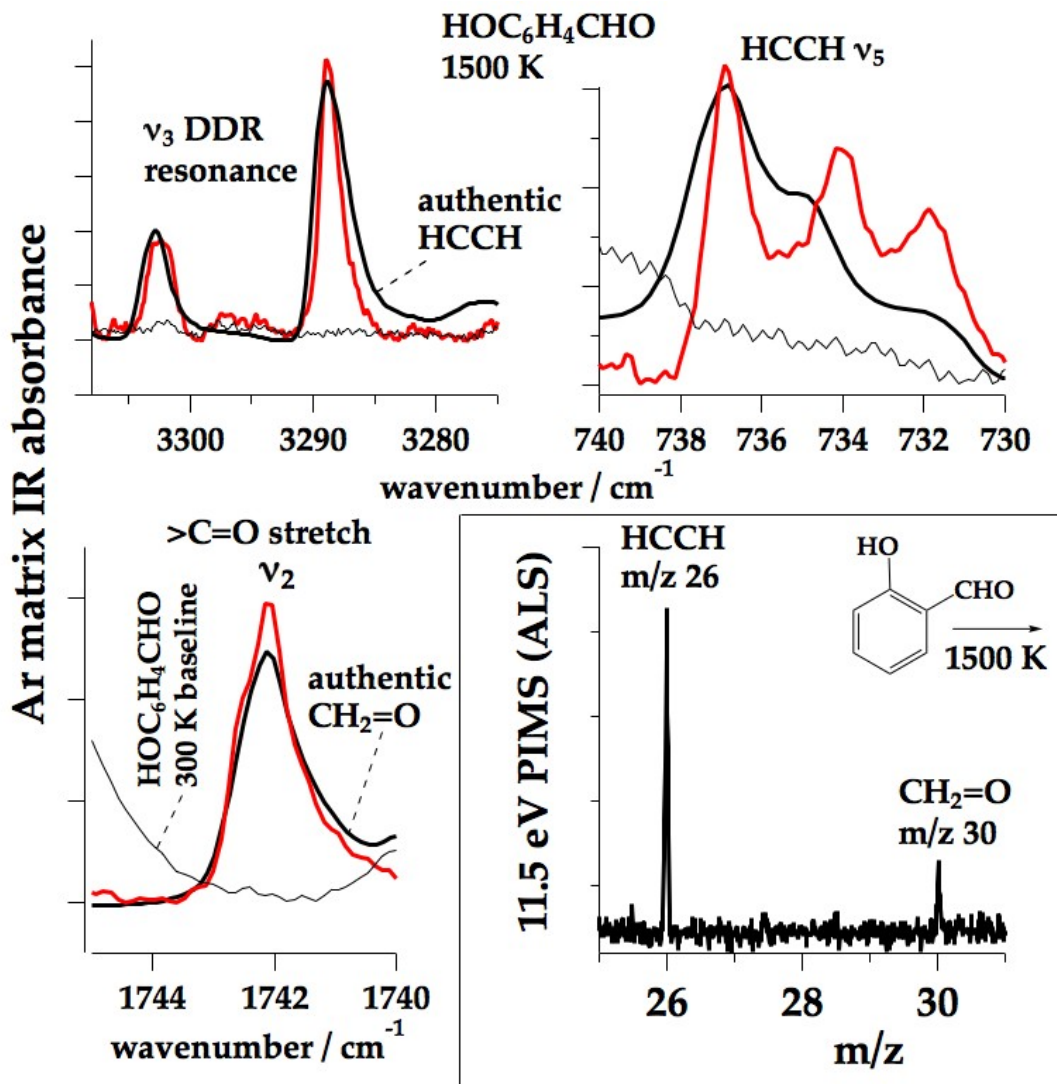


Fig. 11. Heating *o*-HOC₆H₄CHO to 1500 K leads to the production of both HC≡CH and CH₂O. The three Ar matrix IR spectra have a background spectrum of salicylaldehyde deposited at 300 K (thin black line). The solid black lines at the top are authentic samples of acetylene. An authentic sample of formaldehyde is plotted as a solid black line in the bottom IR spectrum. The red traces are the IR spectra that result when salicylaldehyde is subjected to pyrolysis at 1500 K. The presence of HCCH is identified¹⁰⁷ by the presence of the ν_3 DDR resonance and ν_5 . Formaldehyde is detected¹⁰⁸ by the observation of the intense ν_2 (CH₂=O). The PIMS scan in bottom right results from pyrolysis of *o*-HOC₆H₄CHO at 1500 K with the ALS synchrotron tuned to 11.5 eV. The ionization energies of acetylene

and formaldehyde are known to be 11.4 eV and 10.9 eV (see Table 1). Both $\text{HC}\equiv\text{CH}$ and $\text{CH}_2=\text{O}$ are observed at m/z 26 and m/z 30.

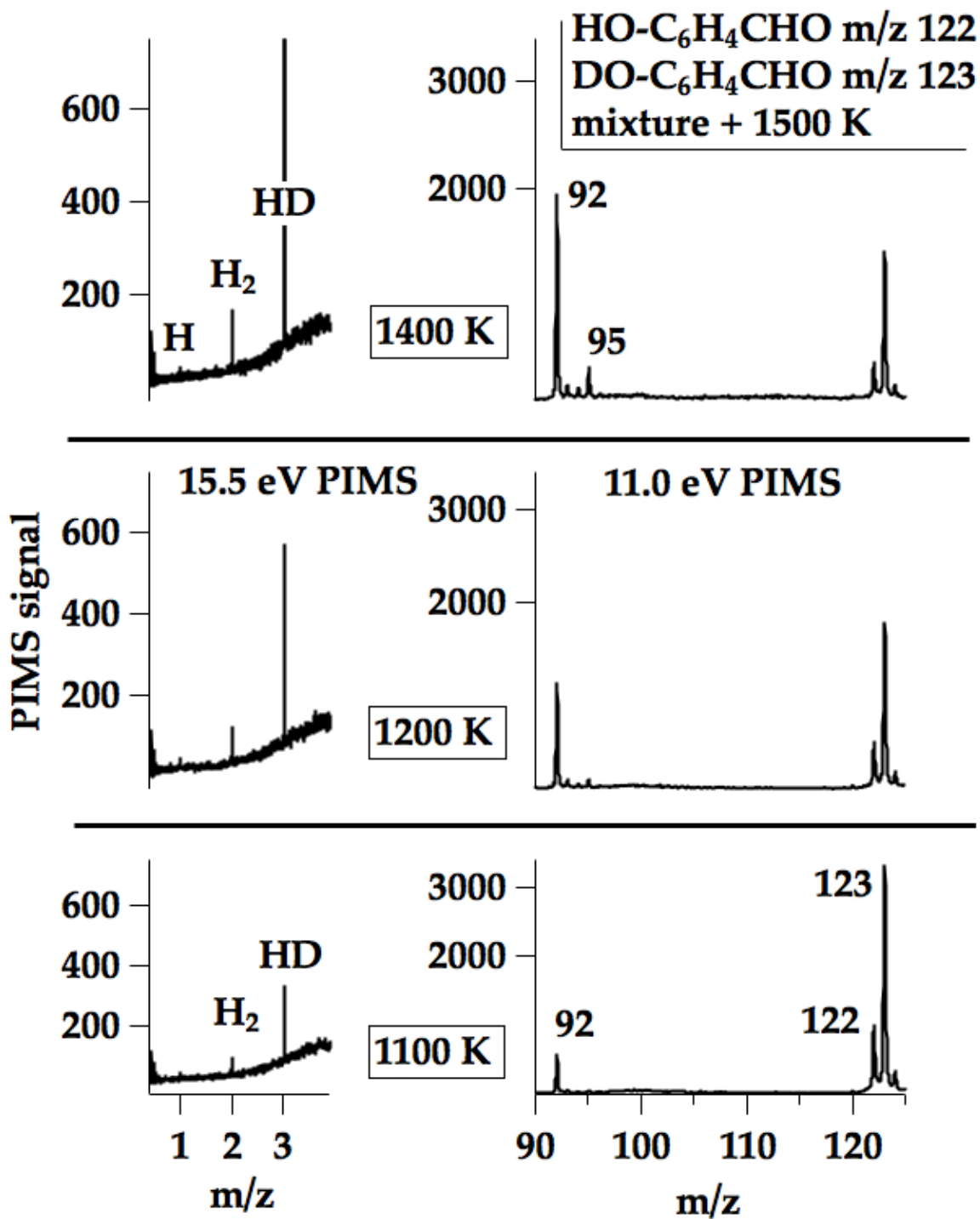


Fig. 12. Left panels: The 15.5 eV PIMS spectra of a mixture of salicylaldehyde-d₁ (m/z 123) and salicylaldehyde-d₀ (m/z 122) diluted in He and passed through a 0.66 mm ID SiC are direct evidence of the functional group interaction mechanism shown in Scheme 6. Intense signal is observed at m/z 2 and 3 from

the elimination of H₂ and HD. There appears to be only a minute amount of H-atoms (m/z 1). The presence of m/z 95 is assigned to phenol-d₁ confirmed by PIE, and m/z 92 is due to C₅H₄=C=O. Trace amounts of m/z 94 (C₆H₅OH) and m/z 93 (¹³C isotope peak of m/z 92) were identified *via* PIE scans.

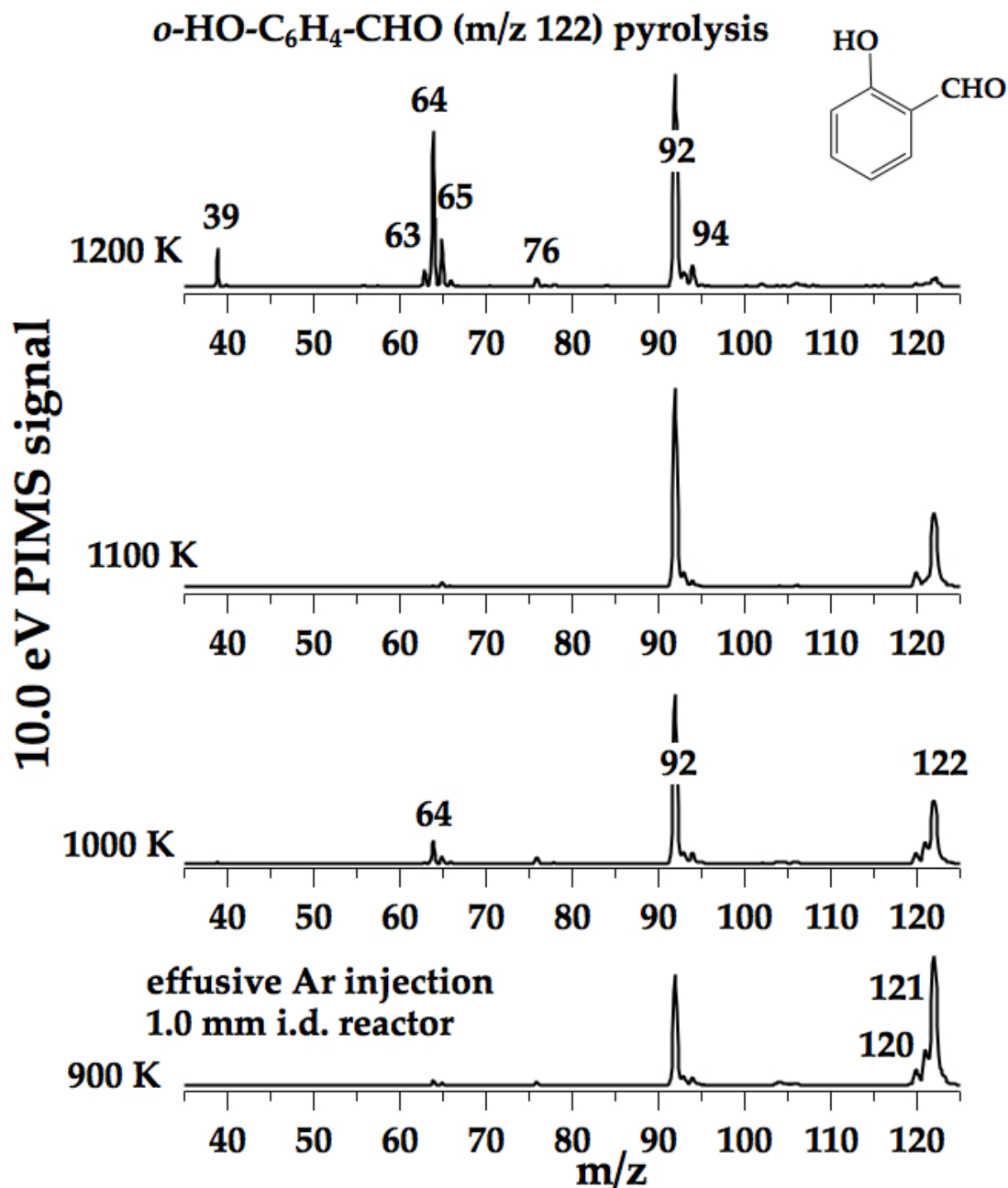


Fig. S1. The SLS synchrotron VUV (10.0 eV) PIMS spectrum of salicylaldehyde diluted (0.1 % or less) in Ar with continuous flow through a 1 mm ID SiC reactor shows signals at m/z 120 (assigned as the keto-carbonyl σ -O=C₆H₄=C=O) and 121 along with m/z 92 (C₅H₄=C=O) and m/z 64 (HC≡C-C≡C-CH₃ or HC≡C-CH=C=CH₂). Further heating generates signals at m/z 39 (HCCCH₂), 63 (C₅H₃), 65 (C₅H₅), 76 (σ -C₆H₄), and 94 (C₆H₅OH).

References

- (1) Rinaldi, R.; Jastrzebski, R.; Clough, M. T.; Ralph, J.; Kennema, M.; Bruijninx, P. C. A.; Weckhuysen, B. M. Paving the Way for Lignin Valorisation: Recent Advances in Bioengineering, Biorefining and Catalysis. *Angew. Chem. Int. Ed.* **2016**, *55*, 8164-8215.
- (2) Nowakowski, D. J.; Bridgwater, A. V.; Elliott, D. C.; Meier, D.; de Wild, P. Lignin Fast Pyrolysis: Results From an International Collaboration. *J. Anal. Appl. Pyrolysis* **2010**, *88*, 53-72.
- (3) Kohse-Höinghaus, K.; Osswald, P.; Cool, T. A.; Kasper, T.; Hansen, N.; Qi, F.; Westbrook, C. K.; Westmoreland, P. R. Biofuel Combustion Chemistry: From Ethanol to Biodiesel. *Angew. Chem. Int. Ed.* **2010**, *49*, 3572-3597.
- (4) Leitner, W.; Klankermayer, J.; Pischinger, S.; Pitsch, H.; Kohse-Höinghaus, K. Advanced Biofuels and Beyond: Chemistry Solutions for Propulsion and Production. *Angew. Chem. Int. Ed.* **2017**, *56*, 5371.
- (5) IPCC. 5th Assessment Report (AR5). **2010**. The *Intergovernmental Panel on Climate Change* makes a compelling case for the extent of climate triggered by CO₂ emissions. Their most recent report is AR5 and can be found at the IPCC website: <http://www.ipcc.ch/>
- (6) Flood, W. E.: *The Dictionary of Chemical Names*; Littlefield, Adams & Co.: Totowa, NJ, 1967. **Lignin** is derived from the L. *lignum* (wood). The name

catechol is derived from catechin + ol denoting a phenol. Catechin is a colorless, crystalline compound present in catechu, an Indian/Burmese tree.

Salicylaldehyde is the aldehyde of salicyl alcohol which is obtained from the bark of the willow tree. The name is derived from Latin salix, salic — willow.

- (7) Boerjan, W.; Ralph, J.; Baucher, M. Lignin Biosynthesis. *Annual Review of Plant Biology* **2003**, *54*, 519-546.
- (8) Vanholme, R.; Demedts, B.; Morreel, K.; Ralph, J.; Boerjan, W. Lignin Biosynthesis and Structure. *Plant Physiology* **2010**, *153*, 895-905.
- (9) Jiang, G. Z.; Nowakowski, D. J.; Bridgwater, A. V. Effect of the Temperature on the Composition of Lignin Pyrolysis Products. *Energy & Fuels* **2010**, *24*, 4470-4475.
- (10) Jiang, G. Z.; Nowakowski, D. J.; Bridgwater, A. V. A Systematic Study of the Kinetics of Lignin Pyrolysis. *Thermochimica Acta* **2010**, *498*, 61-66.
- (11) Patwardhan, P. R.; Brown, R. C.; Shanks, B. H. Product Distribution from the Fast Pyrolysis of Hemicellulose. *ChemSusChem* **2011**, *4*, 636-643.
- (12) Patwardhan, P. R.; Brown, R. C.; Shanks, B. H. Understanding the Fast Pyrolysis of Lignin. *Chemsuschem* **2011**, *4*, 1629-1636.
- (13) Radlein, D.; Piskorz, J.; Scott, D. Lignin Derived Oils from the Fast Pyrolysis of Poplar Wood. *J. Anal. Appl. Pyrolysis* **1987**, *12*, 51-59.

- (14) Robichaud, D. J.; Nimlos, M. R.; Ellison, G. B.: Pyrolysis Mechanisms of Lignin Model Compounds Using a Heated Micro-Reactor. In *Reaction Pathways and Mechanisms in Thermocatalytic Biomass Conversion II*; Zhang, Z. C., Schlaf, M., Eds.; 8; Springer Science+Business Media Singapore: Berlin, (2016); pp 145–171.
- (15) Han, J.; Kim, H. The Reduction and Control Technology of Tar During Biomass Gasification/Pyrolysis: An Overview. *Renewable & Sustainable Energy Reviews* **2008**, *12*, 397-416.
- (16) Bohm, H.; Jander, H. Pah Formation in Acetylene-Benzene Pyrolysis. *Phys. Chem. Chem. Phys.* **1999**, *1*, 3775-3781.
- (17) Kamphus, M.; Braun-Unkhoff, M.; Kohse-Höinghaus, K. Formation of Small PAHs in Laminar Premixed Low-Pressure Propene and Cyclopentene Flames: Experiment and Modeling. *Comb. and Flame* **2008**, *152*, 28-59.
- (18) Sanchez, N. E.; Callejas, A.; Millera, A.; Bilbao, R.; Alzueta, M. U. Influence of the Oxygen Presence on Polycyclic Aromatic Hydrocarbon (PAH) Formation from Acetylene Pyrolysis under Sooting Conditions. *Energy & Fuels* **2013**, *27*, 7081-7088.
- (19) Gasser, C. A.; Hommes, G.; Schaeffer, A.; Corvini, P. F. X. Multi-catalysis reactions: new prospects and challenges of biotechnology to valorize lignin. *Applied Microbiology and Biotechnology* **2012**, *95*, 1115-1134.

- (20) Parsell, T. H.; Owen, B. C.; Klein, I.; Jarrell, T. M.; Marcum, C. L.; Hauptert, L. J.; Amundson, L. M.; Kenttaemaa, H. I.; Ribeiro, F.; Miller, J. T.; Abu-Omar, M. M. Cleavage and hydrodeoxygenation (HDO) of C-O bonds relevant to lignin conversion using Pd/Zn synergistic catalysis. *Chem. Sci.* **2013**, *4*, 806-813.
- (21) Ruiz, G. T.; Juliarena, M. P.; Ferraudi, G.; Lappin, A. G.; Boggess, W.; Feliz, M. R. On the Homogeneous Catalysis of the Photochemical and Thermal O₂-Degrading of Lignin in Aqueous Solution. Mechanistic Observations on the Processes Catalyzed by Al-III(Phthalocyaninetetrasulfonate)³⁻ and Co-III Dimethylglyoximate Complexes. *Polyhedron* **2012**, *38*, 36-43.
- (22) Horn, C.; Roy, K.; Frank, P. Shock-Tube Study on the High-Temperature Pyrolysis of Phenol. *Proc. Comb. Inst.* **1998**, *27*, 321.
- (23) Khachatryan, L.; Adoukpe, J.; Dellinger, B. Formation of Phenoxy and Cyclopentadienyl Radicals from the Gas-Phase Pyrolysis of Phenol. *J. Phys. Chem. A* **2008**, *112*, 481-487.
- (24) Lovell, A. B.; Brezinsky, K.; Glassman, I. The Gas-Phase Pyrolysis of Phenol. *Int. J. Chem. Kinetics* **1989**, *21*, 547-560.
- (25) Scheer, A. M.; Mukarakate, C.; Robichaud, D. J.; Nimlos, M. R.; Carstensen, H.-H.; Ellison, G. B. Unimolecular Thermal Decomposition of Phenol and d₅-Phenol: Direct Observation of Cyclopentadiene Formation via Cyclohexadienone. *J. Chem. Phys.* **2012**, *136*, 044309 (11 pp)

- (26) Arends, I. W. C. E.; Louw, R.; Mulder, P. Kinetic-Study of the Thermolysis of Anisole in a Hydrogen Atmosphere. *J. Phys. Chem.* **1993**, *97*, 7914-7925.
- (27) Friderichsen, A. V.; Shin, E.-J.; Evans, R. J.; Nimlos, M. R.; Dayton, D. C.; Ellison, G. B. The Pyrolysis of Anisole (C₆H₅OCH₃) Using a Hyperthermal Nozzle. *Fuel* **2001**, *80*, 1747-1755.
- (28) Nowakowska, M.; Herbinet, O.; Dufour, A.; Glaude, P.-A. Detailed Kinetic Study of Anisole Pyrolysis and Oxidation to Understand Tar Formation During Biomass Combustion and Gasification. *Comb. and Flame* **2014**, *161*, 1474-1488.
- (29) Scheer, A. M.; Mukarakate, C.; Robichaud, D. J.; Ellison, G. B.; Nimlos, M. R. Radical Chemistry in the Thermal Decomposition of Anisole and Deuterated Anisoles: An Investigation of Aromatic Growth. *J. Phys. Chem. A* **2010**, *114*, 9043-9056.
- (30) Suryan, M. M.; Kafafi, S. A.; Stein, S. E. Dissociation of Substituted Anisoles - Substituent Effects on Bond Strengths. *J. Am. Chem. Soc.* **1989**, *111*, 4594-4600.
- (31) Suryan, M. M.; Kafafi, S. A.; Stein, S. E. The Thermal-Decomposition of Hydroxy-Substituted and Methoxy-Substituted Anisoles. *J. Am. Chem. Soc.* **1989**, *111*, 1423-1429.

- (32) Grela, M. A.; Colussi, A. J. Kinetics and Mechanism of the Thermal Decomposition of Unsaturated Aldehydes: Benzaldehyde, 2-Butenal, and 2-Furaldehyde. *The Journal of Physical Chemistry* **1986**, *90*, 434-437.
- (33) Vasiliou, A. K.; Kim, J. H.; Ormond, T. K.; Piech, K. M.; Urness, K. N.; Scheer, A. M.; Robichaud, D. J.; Mukarakate, C.; Nimlos, M. R.; Daily, J. W.; Guan, Q.; Carstensen, H.-H.; Ellison, G. B. Biomass Pyrolysis: Thermal Decomposition Mechanisms of Furfural and Benzaldehyde *J. Chem. Phys.* **2013**, *139*, 104310 (11 pp)
- (34) Scheer, A. M.; Mukarakate, C.; Robichaud, D. J.; Nimlos, M. R.; Ellison, G. B. Thermal Decomposition Mechanisms of the Methoxyphenols: Formation of Phenol, Cyclopentadienone, Vinylacetylene, and Acetylene. *J. Phys. Chem. A* **2011**, *115*, 13381-13389.
- (35) Custodis, V. B. F.; Hemberger, P.; Ma, Z.; van Bokhoven, J. A. Mechanism of Fast Pyrolysis of Lignin: Studying Model Compounds. *Journal of Physical Chemistry B* **2014**, *118*, 8524-8531.
- (36) Dorrestijn, E.; Mulder, P. The Radical-Induced Decomposition of 2-Methoxyphenol. *J. Chem. Soc. – Perkin Trans. 2* **1999**, 777-780.
- (37) Robichaud, D. J.; Scheer, A. M.; Mukarakate, C.; Ormond, T. K.; Buckingham, G. T.; Ellison, G. B.; Nimlos, M. R. Unimolecular Thermal Decomposition of Dimethoxybenzenes. *J. Chem. Phys.* **2014**, *140*, 234302 – 234316.

- (38) Asmadi, M.; Kawamoto, H.; Saka, S. Thermal Reactions of Guaiacol and Syringol as Lignin Model Aromatic Nuclei. *J. Anal. Appl. Pyrolysis* **2011**, *92*, 88-98.
- (39) Asmadi, M.; Kawamoto, H.; Saka, S. The Effects of Combining Guaiacol and Syringol on their Pyrolysis. *Holzforschung* **2012**, *66*, 323-330.
- (40) Scheer, A. M. *Thermal Decomposition Mechanisms of Lignin Model Compounds: From Phenol to Vanillin*. PhD Thesis, University of Colorado, 2011.
- (41) Shin, E. J.; Nimlos, M. R.; Evans, R. J. A Study of the Mechanisms of Vanillin Pyrolysis by Mass Spectrometry and Multivariate Analysis. *Fuel* **2001**, *80*, 1689-1696.
- (42) Pilling, M. J. Reactions of Hydrocarbon Radicals and Biradicals. *J. Phys. Chem. A* **2013**, *117*, 3697-3717.
- (43) Vasiliou, A. K.; Piech, K. M.; Reed, B.; Zhang, X.; Nimlos, M. R.; Ahmed, M.; Golan, A.; Kostko, O.; Osborn, D. L.; Urness, K. N.; David, D. E.; Daily, J. W.; Stanton, J. F.; Ellison, G. B. Thermal Decomposition of CH₃CHO Studied by Matrix Infrared Spectroscopy and Photoionization Mass Spectroscopy *J. Chem. Phys.* **2012**, *137*, 164308. (14 pp)
- (44) Urness, K. N.; Guan, Q.; Golan, A.; Daily, J. W.; Nimlos, M. R.; Stanton, J. F.; Ahmed, M.; Ellison, G. B. Pyrolysis of Furan in a Microreactor *J. Chem. Phys.* **2013**, *139*, 124305-124314

- (45) Zhang, X.; Friderichsen, A. V.; Nandi, S.; Ellison, G. B.; David, D. E.; McKinnon, J. T.; Lindeman, T. G.; Dayton, D. C.; Nimlos, M. R. Intense, Hyperthermal Source of Organic Radicals for Matrix-Isolation Spectroscopy. *Rev. Sci. Inst.* **2003**, *74*, 3077-3086.
- (46) Mukarakate, C.; Scheer, A. M.; Robichaud, D. J.; Jarvis, M. W.; David, D. E.; Ellison, G. B.; Nimlos, M. R.; Davis, M. F. Laser Ablation with Resonance-Enhanced Multiphoton Ionization Time-of-Flight Mass Spectrometry for Determining Aromatic Lignin Volatilization Products from Biomass. *Rev. Sci. Inst.* **2011**, *82*, 33104-33114.
- (47) Guan, Q.; Urness, K. N.; Ormond, T. K.; David, D. E.; Ellison, G. B.; Daily, J. W. The Properties of a Micro-Reactor for the Study of the Unimolecular Decomposition of Large Molecules. *Int. Rev. Phys. Chem.* **2014**, *33*, 447-487.
- (48) Ormond, T. K.; Scheer, A. M.; Nimlos, M. R.; Robichaud, D. J.; Daily, J. W.; Stanton, J. F.; Ellison, G. B. Polarized Matrix Infrared Spectra of Cyclopentadienone: Observations, Calculations, and Assignment for an Important Intermediate in Combustion and Biomass Pyrolysis. *J. Phys. Chem. A* **2014**, *118*, 708-718.
- (49) Lockyer, N. P.; Vickerman, J. C. Single Photon Ionisation Mass Spectrometry Using Laser-Generated Vacuum Ultraviolet Photons. *Laser Chem.* **1997**, *17*, 139-159.

- (50) McLafferty, F. W.: *Interpretation of Mass Spectra*; Third ed.; University Science Books: Mill Valley, CA 94941, 1980.
- (51) McLoughlin, R. G.; Traeger, J. C. Photo-Ionization Study of Some Benzoyl Compounds - Thermochemistry of $[C_7H_5O]^+$ Formation. *Journal of Mass Spectrometry* **1979**, *14*, 434-438.
- (52) Palmer, M. H.; Moyes, W.; Speirs, M.; Ridyard, J. N. A. Electronic-Structure of Substituted Benzenes - *ab Initio* Calculations and Photoelectron Spectra for Phenol, the Methyl-Derivatives and Fluoro-Derivatives, and the Dihydroxybenzenes. *J. Mol. Struct.* **1979**, *52*, 293-307. (See Fig. 4)
- (53) Foffani, A.; Cantone, B.; Pignataro, S.; Grasso, F. Ionization Potentials and Substituent Effects for Aromatic Carbonyl Compounds. *Zeitschrift Fur Physikalische Chemie* **1964**, *42*, 221.
- (54) Heimann, P. A.; Koike, M.; Hsu, C. W.; Blank, D.; Yang, X. M.; Suits, A. G.; Lee, Y. T.; Evans, M.; Ng, C. Y.; Flaim, C.; Padmore, H. A. Performance of the Vacuum Ultraviolet High-Resolution and High-Flux Beamline for Chemical Dynamics Studies at the Advanced Light Source. *Rev. Sci. Inst.* **1997**, *68*, 1945-1951.
- (55) Suits, A. G.; Heimann, P.; Yang, X. M.; Evans, M.; Hsu, C. W.; Lu, K. T.; Lee, Y. T.; Kung, A. H. A Differentially Pumped Harmonic Filter on the Chemical-Dynamics Beamline at the Advanced Light-Source. *Rev. Sci. Inst.* **1995**, *66*, 4841-4844.

- (56) Cool, T. A.; Wang, J.; Nakajima, K.; Taatjes, C. A.; McIlroy, A. Photoionization Cross Sections for Reaction Intermediates in Hydrocarbon Combustion. *Int. J. Mass Spectrom.* **2005**, *247*, 18-27.
- (57) Wang, J.; Yang, B.; Cool, T. A.; Hansen, N.; Kasper, T. Near-Threshold Absolute Photoionization Cross-Sections of Some Reaction Intermediates in Combustion. *Int. J. Mass Spectrom.* **2008**, *269*, 210-220.
- (58) Wang, J.; Yang, B.; Cool, T. A.; Hansen, N. Absolute Cross-Sections for Dissociative Photoionization of Some Small Esters. *Int. J. Mass Spectrom.* **2010**, *292*, 14-22.
- (59) Bodi, A.; Sztaray, B.; Baer, T.; Johnson, M.; Gerber, T. Data Acquisition Schemes for Continuous Two-Particle Time-of-Flight Coincidence Experiments. *Rev. Sci. Inst.* **2007**, *78*, 084102 - 084109.
- (60) Bodi, A.; Johnson, M.; Gerber, T.; Gengeliczki, Z.; Sztaray, B.; Baer, T. Imaging Photoelectron Photoion Coincidence Spectroscopy with Velocity Focusing Electron Optics. *Rev. Sci. Inst.* **2009**, *80*, 034101-034108.
- (61) Johnson, M.; Bodi, A.; Schulz, L.; Gerber, T. Vacuum Ultraviolet Beamline at the Swiss Light Source for Chemical Dynamics Studies. *Nuclear Instruments & Methods in Physics Research Section A-Accelerators Spectrometers Detectors and Associated Equipment* **2009**, *610*, 597-603.

- (62) Bödi, A.; Hemberger, P.; Gerber, T.; Sztaray, B. A New Double Imaging Velocity Focusing Coincidence Experiment: i^2 PEPICO. *Rev. Sci. Inst.* **2012**, *83*, 083105-083112.
- (63) See Supplementary Material Document No. _____ for . The SLS synchrotron VUV (10.0 eV) PIMS spectrum of salicylaldehyde.
- (64) Blanksby, S. J.; Ellison, G. B. Bond Dissociation Energies of Organic Molecules. *Acct. Chem. Res.* **2003**, *36*, 255-263.
- (65) Hemberger, P.; da Silva, G.; Trevitt, A. J.; Gerber, T.; Bodi, A. Are the Three Hydroxyphenyl Radical Isomers Created Equal? - The Role of the Phenoxy Radical. *Phys. Chem. Chem. Phys.* **2015**, *17*, 30076-30083.
- (66) Zhang, X.; Maccarone, A. T.; Nimlos, M. R.; Kato, S.; Bierbaum, V. M.; Ellison, G. B.; Ruscic, B.; Simmonett, A. C.; Allen, W. D.; Schaefer, H. F. Unimolecular Thermal Fragmentation of *ortho*-Benzyne. *J. Chem. Phys.* **2007**, *126*, 044312 - 044322.
- (67) Hemberger, P.; Custodis, V. B. F.; Bodi, A.; Gerber, T.; van Bokhoven, J. A. Understanding the Mechanism of Catalytic Fast Pyrolysis by Unveiling Reactive Intermediates in Heterogeneous Catalysis. *Nat. Commun.* **2017**.
- (68) Lomnicki, S.; Truong, H.; Dellinger, B. Mechanisms of Product Formation from the Pyrolytic Thermal Degradation of Catechol. *Chemosphere* **2008**, *73*, 629-633.

- (69) Yang, H. M.; Furutani, Y.; Kudo, S.; Hayashi, J.; Norinaga, K. Experimental Investigation of Thermal Decomposition of Dihydroxybenzene Isomers: Catechol, Hydroquinone, and Resorcinol. *J. Anal. Appl. Pyrolysis* **2016**, *120*, 321-329.
- (70) Khachatryan, L.; Adoukpe, J.; Asatryan, R.; Dellinger, B. Radicals from the Gas-Phase Pyrolysis of Catechol: 1. *o*-Semiquinone and *ipso*-Catechol Radicals. *J. Phys. Chem. A* **2010**, *114*, 2306-2312.
- (71) Khachatryan, L.; Asatryan, R.; McFerrin, C.; Adoukpe, J.; Dellinger, B. Radicals from the Gas-Phase Pyrolysis of Catechol. 2. Comparison of the Pyrolysis of Catechol and Hydroquinone. *J. Phys. Chem. A* **2010**, *114*, 10110-10116.
- (72) Altarawneh, M.; Dlugogorski, B. Z.; Kennedy, E. M.; Mackie, J. C. Theoretical Study of Unimolecular Decomposition of Catechol. *J. Phys. Chem. A* **2010**, *114*, 1060-1067.
- (73) Ichino, T.; Wren, S. W.; Vogelhuber, K. M.; Gianola, A. J.; Lineberger, W. C.; Stanton, J. F. The Vibronic Level Structure of the Cyclopentadienyl Radical. *J. Chem. Phys.* **2008**, *129*, 084310.
- (74) Kidwell, N. M.; Vaquero-Vara, V.; Ormond, T. K.; Buckingham, G. T.; Zhang, D.; Mehta-Hurt, D. N.; McCaslin, L.; Nimlos, M. R.; Daily, J. W.; Dian, B. C.; Stanton, J. F.; Ellison, G. B.; Zwier, T. S. Chirped-Pulse Fourier Transform Microwave Spectroscopy Coupled with a Hyperthermal Reactor: Structural

- Determination of the Reactive Intermediate Cyclopentadienone. *J. Phys. Chem. Letts.* **2014**, *5*, 2201-2207.
- (75) Ormond, T. K.; Scheer, A. M.; Nimlos, M. R.; Robichaud, D. J.; Troy, T. P.; Ahmed, M.; Daily, J. W.; Stanton, J. F.; Ellison, G. B. Pyrolysis of Cyclopentadienone: Mechanistic Insights From a Direct Measurement of Product Branching Ratios *J. Phys. Chem. A* **2015**, *119*, 7222-7234.
- (76) Ormond, T. K.; Hemberger, P.; Troy, T. P.; Ahmed, M.; Stanton, J. F.; Ellison, G. B. The Ionization Energy of Cyclopentadienone: A Photoelectron-Photoion Coincidence Study. *Molecular Physics* **2015**, *113*, 2350-2358.
- (77) Khuseynov, D.; Stanton, J. F.; Sanov, A. Low-Lying Electronic States of Cyclopentadienone. *J. Phys. Chem. A* **2014**, *118*, 6965-6970.
- (78) Palenius, H. P.; Kohl, J. L.; Parkinson, W. H. Absolute Measurement of Photoionization Cross-Section of Atomic-Hydrogen with a Shock-Tube for Extreme Ultraviolet. *Physical Review A* **1976**, *13*, 1805-1816.
- (79) Glass-Maujean, M.; Klumpp, S.; Werner, L.; Ehresmann, A.; Schmoranzner, H. Cross Sections for the Ionization Continuum of H₂ in the 15.3-17.2 eV Energy Range. *J. Chem. Phys.* **2007**, *126*.
- (80) The salicylaldehyde decomposition temperatures vary with the properties of different micro-reactors. This is because the hydrodynamic state of the gases is different in a pulsed reactor (Fig. 1) or the continuous reactors (Fig. 2 and

Fig. S1). The thermal conductivity of He is dramatically different than that of Ar. We have employed four different reactors in this study; Fig. 1 is a pulsed, He reactor, Fig. 2 is a continuous He reactor, Fig. S1 is a continuous Ar reactor, and all the IR spectra result from pyrolysis in a pulsed Ar reactor. The IR spectra and PIMS in Figs. 1 and S1 are produced by a 1 mm i.d. SiC reactor; the PIMS in Fig. 2 uses a 0.66 mm i.d. SiC reactor. The proper modeling of these 4 different reactors will require the techniques of Guan, *et al.* (ref. 47) and is beyond the scope of this paper.

- (81) da Silva, G.; Bozzelli, J. W. Benzoyl Radical Decomposition Kinetics: Formation of Benzaldehyde + H, Phenyl + CH₂O, and Benzene+ HCO. *J. Phys. Chem. A* **2009**, *113*, 6979-6986.
- (82) Baulch, D. L.; Cobos, C. J.; Cox, R. A.; Esser, C.; Frank, P.; Just, T.; Kerr, J. A.; Pilling, M. J.; Troe, J.; Walker, R. W.; Warnatz, J. Evaluated Kinetic Data for Combustion Modeling. *J. Phys. Chem. Ref. Data* **1992**, *21*, 411-734.
- (83) Benson, S. W.; Shaw, R. Kinetics and Mechanism of Pyrolysis of 1,4-Cyclohexadiene. *Trans. Faraday Soc.* **1967**, *63*, 985-992.
- (84) Asatryan, R.; Ruckenstein, E. Dihydrogen Catalysis: A Remarkable Avenue in the Reactivity of Molecular Hydrogen. *Catalysis Reviews-Science and Engineering* **2014**, *56*, 403-475.

- (85) Mulcahy, M. F. R.; Tucker, B. G.; Williams, D. J.; Wilmshur, J. R. Decomposition and Rearrangement of Free Radicals from Alkyl Phenyl Ethers. *Chem. Comm.* **1965**, 609-610.
- (86) Mulcahy, M. F. R.; Tucker, B. G.; Williams, D. J.; Wilmshur, J. R. Reactions of Free Radicals with Aromatic Compounds in Gaseous Phase 3. Kinetics of Reaction of Methyl Radicals with Anisole (Methoxybenzene). *Australian Journal of Chemistry* **1967**, *20*, 1155-1171.
- (87) Porterfield, J. P. *The Thermal Decomposition of Biofuels in a Heated Micro-Reactor: Ketones, Carbohydrates, and Esters*. PhD Thesis, University of Colorado, 2016.
- (88) Urness, K. N.; Guan, Q.; Troy, T. P.; Ahmed, M.; Daily, J. W.; Ellison, G. B.; Simmie, J. M. Pyrolysis Pathways for the Furanic Ether, 2-Methoxyfuran. *J. Phys. Chem. A* **2015**, *119*, 9962-9977.
- (89) Pedley, J. B.; Naylor, R. D.; Kirby, S. P.: *Thermochemistry of Organic Compounds*; 2 ed.; Chapman and Hall: New York, 1986.
- (90) Ribeiro da Silva, M. D. M. C.; Ribeiro da Silva, M. A. V.; Pilcher, G. Enthalpies of Combustion of 1,2-Dihydroxybenzene and of 6-Alkylsubstituted 1,2-Dihydroxybenzenes. *J. Chem. Thermodynamics* **1984**, *16*, 1149-1155.

- (91) Riberio da Silva, M. D. M. C.; Araujo, N. R. M. Thermochemical Studies on Salicylaldehyde and Salicylamide. *J. Chem. Thermodynamics* **2007**, *39*, 1372-1376.
- (92) Ribeiro da Silva, M. D. M. C.; Goncalves, M. V.; Monte, M. J. S. Thermodynamic Study on Hydroxybenzaldehyde Derivatives: 3-and 4-Hydroxybenzaldehyde Isomers and 3,5-Di-tert-Butyl-2-Hydroxybenzaldehyde. *J. Chem. Thermodynamics* **2010**, *42*, 472-477.
- (93) Nix, M. G. D.; Devine, A. L.; Cronin, B.; Dixon, R. N.; Ashfold, M. N. R. High Resolution Photofragment Translational Spectroscopy Studies of the Near Ultraviolet Photolysis of Phenol. *J. Chem. Phys.* **2006**, *125*, 133318-133331.
- (94) King, G. A.; Oliver, T. A. A.; Dixon, R. N.; Ashfold, M. N. R. Vibrational Energy Redistribution in Catechol During Ultraviolet Photolysis. *Phys. Chem. Chem. Phys.* **2012**, *14*, 3338-3345.
- (95) Liu, J. J.; Salumbides, E. J.; Hollenstein, U.; Koelemeij, J. C. J.; Eikema, K. S. E.; Ubachs, W.; Merkt, F. Determination of the Ionization and Dissociation Energies of the Hydrogen Molecule. *J. Chem. Phys.* **2009**, *130*.
- (96) Sprecher, D.; Liu, J. J.; Jungen, C.; Ubachs, W.; Merkt, F. Communication: The Ionization and Dissociation Energies of HD. *J. Chem. Phys.* **2010**, *133*, 111102 (4 pp)

- (97) Lipert, R. J.; Colson, S. D. Time-Resolved Pump Probe Photoionization Study of Excited-State Dynamics of Phenol (H₂O)₂ and Phenol (H₂O)₃. *J. Phys. Chem.* **1990**, *94*, 2358-2361.
- (98) Pratt, S. T.; Dehmer, P. M.; Dehmer, J. L. Zero-Kinetic-Energy Photoelectron-Spectroscopy from the \tilde{a}^1A_u State of Acetylene - Renner-Teller Interactions in the *Trans*-Bending Vibration of C₂H₂⁺ X ²Π_u. *J. Chem. Phys.* **1993**, *99*, 6233-6244.
- (99) Schulenburg, A. M.; Meisinger, M.; Radi, P. P.; Merkt, F. The Formaldehyde Cation: Rovibrational Energy Level Structure and Coriolis Interaction Near the Adiabatic Ionization Threshold. *J. Mol. Spectrosc.* **2008**, *250*, 44-50.
- (100) Kim, J. B.; Yacovitch, T. I.; Hock, C.; Neumark, D. M. Slow Photoelectron Velocity-Map Imaging Spectroscopy of the Phenoxide and Thiophenoxide Anions. *Phys. Chem. Chem. Phys.* **2011**, *13*, 17378-17383.
- (101) Weichman, M. L.; Kim, J. B.; Neumark, D. M. Slow Photoelectron Velocity-Map Imaging Spectroscopy of the *ortho*-Hydroxyphenoxide Anion. *J. Phys. Chem. A* **2015**, *119*, 6140-6147.
- (102) Huang, D. L.; Liu, H. T.; Ning, C. G.; Wang, L. S. Vibrational State-Selective Autodetachment Photoelectron Spectroscopy from Dipole-Bound States of Cold 2-Hydroxyphenoxide: *o*-HO(C₆H₄)O. *J. Chem. Phys.* **2015**, *142*, 124309.
(10 pages)

- (103) Zhu, G. Z.; Huang, D. L.; Wang, L. S. Conformation-Selective Resonant Photoelectron Imaging from Dipole-Bound States of Cold 3-Hydroxyphenoxide. *J. Chem. Phys.* **2017**, *147*.
- (104) Matsen, F. A.; Ginsburg, N.; Robertson, W. W. The near Ultraviolet Absorption Spectrum of Phenol Vapor. *J. Chem. Phys.* **1945**, *13*, 309-316.
- (105) Bist, H. D.; Brand, J. C. D.; Williams, D. R. The 2750-Å Electronic Band System of Phenol Part 1. In-Plane Vibrational Spectrum. *J. Mol. Spectrosc.* **1966**, *21*, 76-98.
- (106) Bist, H. D.; Brand, J. C. D.; Williams, D. R. The 2750-Å Band System of Phenol Part 2. Extended Vibrational Assignments and Band Contour Analysis. *J. Mol. Spectrosc.* **1967**, *24*, 413-467.
- (107) Of the 5 modes of $\text{HC}\equiv\text{CH}$, only the asymmetric CH stretch, $\sigma_u \nu_3$, and the asymmetric HCCH bend, $\pi_u \nu_5$, are IR active. In the gas-phase ν_3 HCCH is observed at 3294.9 cm^{-1} and 3281.9 cm^{-1} and is split by a Darling-Dennison resonance (DDR) of 13 cm^{-1} . In an Ar matrix, ν_3 shifts to 3302 cm^{-1} and 3288 cm^{-1} ; the DDR is 14 cm^{-1} in the cryogenic matrix. The gas phase value for ν_5 is 730.3 cm^{-1} and shifts to 736.8 cm^{-1} in an Ar matrix.
- (108) The 6 modes of formaldehyde as observed in an Ar matrix are: ν_1 (a_1 , CH_2 sym st) = 2798 cm^{-1} , ν_2 (a_1 , CO st) = 1742 cm^{-1} , ν_3 (a_1 , CH_2 scis) = 1499 cm^{-1} , ν_4 (b_1 , CH_2 umbrella) = 1169 cm^{-1} , ν_5 (b_2 , CH_2 a-st) = 2864 cm^{-1} , ν_6 (b_2 , CH_2 rock) = 1245 cm^{-1} .

